NASA Technical Memorandum 4096

The NASA Langley Laminar-Flow-Control Experiment on a Swept, Supercritical Airfoil

Drag Equations

Cuyler W. Brooks, Jr., Charles D. Harris, and William D. Harvey
Langley Research Center
Hampton, Virginia

National Aeronautics and Space Administration
Office of Management
Scientific and Technical Information Division

1989

Summary

The Langley Research Center has designed a swept, supercritical airfoil incorporating laminar-flow control (LFC) for testing at transonic speeds. Analytical expressions have been developed and an evaluation has been made of the experimental section drag, composed of suction drag and wake drag, by using theoretical design information and experimental data.

The analysis shows that, although the sweep-induced boundary-layer cross-flow influence on the wake drag is too large to be ignored and there is not a practical method for evaluating these cross-flow effects on the experimental wake data, the conventional unswept two-dimensional wake drag computation used in the reduction of the experimental data is at worst 10 percent too high.

Introduction

The total drag of laminar-flow-control airfoils may be determined by combining the measured suction power (suction drag), required to maintain a laminar boundary layer, with the measured stagnation pressure losses in the wake just downstream of the trailing edge (wake drag). The combination of the two drag forces (wake drag + suction drag) thus represents both the resistance of the air through which the airfoil moves and the penalty incurred in creating a suction flow through the airfoil surface. This total drag must be less than the wake drag of a comparable nonsuction airfoil in order to justify the use of boundary-layer suction.

The suction drag is derived from considerations relating to the power required to create suction through the airfoil surface. It is not an actual physical drag acting to oppose the motion of the airfoil through the air, but a drag computed from suction power requirements. Not considered in the analysis presented in this paper are the penalties due to the weight and maintenance of the suction apparatus and the inefficiency of the suction compressor.

The axisymmetric suction nozzle used in these tests was developed by Dr. Werner Pfenninger during early laminar-flow-control research. The profile shape of the nozzle and the calibration curve for this nozzle, given in the appendix, were communicated informally by Dr. Pfenninger during the design phase of these investigations. The original derivation of the equation for suction drag (eq. (13)) is also due to Dr. Pfenninger.

The wake drag may be determined either by the integration of momentum deficits across the wake as computed from measured wake-rake pressures in the conventional manner of references 1 and 2, for two-dimensional airfoils, or by more sophisticated methods that account for the airfoil sweep by analysis of the airfoil theoretical boundary layer. When the trailing edge is swept, the conventional wake-rake drag computation can be in error because of either inviscid cross-flow (defined as the deviation of the boundary-layer edge flow from the streamwise direction) effects or viscous cross-flow (deviation of flow in the boundary layer from the edge direction) effects (refs. 3 to 6). Therefore, an error analysis of the wake drag is required for swept airfoils, since the mass-flow rate on which the momentum deficit is based can be affected by boundary-layer cross flow and resulting pressure gradients.

The object of this report is the development and application of analytical methods for the evaluation of the coefficients of suction and wake drag for the slotted and porous laminar-flow-control (LFC) airfoils that have been tested in the Langley 8-Foot Transonic Pressure Tunnel (8-ft TPT) at transonic speeds over a range of chord Reynolds numbers. An overview of these experiments is presented in reference 7, and basic experimental results for the slotted configuration are presented in reference 8.

Even though the conventional wake-rake drag computation method does not take into account cross-flow effects, it was the method used to compute wake drag from experimental measurements in the LFC experiment of reference 8. Drag computations based on the theoretical boundary layer on a swept airfoil are evaluated and presented as an indication of the magnitude of the cross-flow effect.

Symbols

b	airfoil span, measured perpendicular to tunnel centerline
b_N	airfoil span, measured along airfoil sweep line
C_p	local pressure coefficient, $(p - p_\infty)/q_\infty$
C_Q	nondimensional local suction coefficient, $-(\rho w)_{ws}/(\rho U)_\infty$
c	airfoil chord, measured parallel to tunnel centerline
c_d	section drag coefficient
$c_{d,s}$	suction drag coefficient
$c_{d,W}$	wake drag coefficient
$c_{d,\text{total}}$	total drag coefficient, $c_{d,s} + c_{d,W}$

c_l	section lift coefficient
c_N	airfoil chord, measured normal to airfoil leading edge
c_p	specific heat at constant pressure
c_v	specific heat at constant volume
D	drag
D_s	suction drag
d	diameter
F	area of duct in plane perpendicular to suction nozzle axis
f	cross-sectional area of nozzle throat, $\pi d_N^2/4$
H	boundary-layer shape factor, δ^*/θ
L_s	suction power, $\frac{\text{ft-lb}}{\text{sec}}$
M	Mach number
m	mass, slugs
$\dot{m}$	mass flow, slugs/sec
p	pressure, psf
q	dynamic pressure, psf
R	gas constant, $c_p - c_v$
R_c	free-stream Reynolds number based on chord
R_d	Reynolds number based on suction-nozzle throat diameter
S	airfoil surface area, bc
s	distance along surface
T	temperature, °R
$\Delta T_{t,sc}$	temperature rise of suction process (eq. (5))
U	velocity component in free-stream direction (in X-direction)
u	velocity component normal to leading edge (in x-direction), $U \cos \Lambda$
v	velocity component parallel to leading edge (in y-direction), $U \sin \Lambda$
W	velocity component perpendicular to free-stream direction (in Z-direction)
w	velocity component in z-direction
α_N	suction-nozzle flow coefficient
γ	ratio of specific heats, c_p/c_v (1.4 for air)
Δ	incremental amount
δ^*	boundary-layer displacement thickness
θ	boundary-layer momentum thickness
Λ	sweep angle
ρ	density

See figures 2 and 4 for geometric orientation of following coordinates:

X	coordinate in flow direction parallel to tunnel centerline
x	coordinate perpendicular to leading edge
Y	coordinate orthogonal to X in airfoil reference plane, positive up
y	coordinate parallel to leading edge, positive up
Z	coordinate orthogonal to X and Y
z	coordinate orthogonal to x and y (also used for local surface normal, positive out from surface)

Subscripts:

e	potential flow at boundary-layer edge
i	ith term
N	nozzle or normal
p	boundary-layer velocities parallel to free-stream direction at boundary-layer edge
s	suction
sc	suction chamber
t	stagnation condition
total	combined suction and wake effect

tr	boundary-layer transition
u, v	boundary-layer thickness definition velocities (eqs. (19b) and (32))
W	wake
W.R.	evaluation at the wake-rake position, $X/c = 1.094$
ws	airfoil surface
∞	free stream

Abbreviations:

L.E.	leading edge
T.E.	trailing edge
LFC	laminar-flow control
TPT	Transonic Pressure Tunnel
2-D	two-dimensional

Experimental Apparatus and Model

A sketch of the LFC airfoil configuration, which incorporates laminar-flow control into an advanced supercritical airfoil, and the shock-free design pressure distribution for this profile are shown in figure 1. The three types of boundary-layer instabilities that were taken into account during the design process are noted on the figure. This airfoil has a nearly full-chord discrete suction surface with an internal suction-flow ducting system. The continuous surface suction as modeled in the design theory can be approached only asymptotically by the actual suction surface of the wind-tunnel model. For the LFC experiment in the 8-ft TPT (ref. 7), two suction surfaces were evaluated: one with narrow (about 0.003 in.), closely spaced spanwise slots and one with spanwise strips of perforated titanium about 0.5 in. wide and 0.4 in. apart (see fig. 2(c)). The slotted surface suction concepts are discussed in more detail in references 7, 8, and 9, and the porous surface suction concept is discussed in reference 10. Sketches of the design laminar regions for these LFC airfoils are shown in figure 2. The laminar regions are bounded by turbulent wedges that develop on the airfoil; these wedges are generated by the junctures of the tunnel liner wall and the airfoil. Suction extends rearward to $X/c = 0.96$ on the slotted-upper-surface airfoil and to $X/c = 0.89$ on the porous-upper-surface airfoil. On the lower surface, only slotted suction was used; the suction extends from near the leading edge to $X/c = 0.842$. The model was mounted vertically in the wind tunnel with 23° of sweep and spanned the test section from ceiling to floor.

Figure 3 shows the chordwise suction distributions theoretically determined to maintain full-chord laminar flow over a range of Reynolds numbers for the upper and lower airfoil surfaces. The theoretical suction distribution for the design case ($M_\infty = 0.82$, $R_c = 20 \times 10^6$)—derived from a linear, parallel, incompressible boundary-layer stability analysis (refs. 11, 12, and 13)—is also presented in table I along with the corresponding suction drag. The theoretical chordwise pressure distribution (fig. 1) was used as input to boundary-layer stability codes to determine these suction requirements. The expressions used to compute the suction drag attributable to either a theoretical or an experimental suction distribution are derived in a following section.

Discussion of Analytical Methods

In order to analyze suction and wake drag, the swept LFC airfoil is considered to have constant cross section and infinite span in steady transonic flow. The local suction velocity through the surface is assumed to be constant along sweep lines parallel to the leading edge. The flow field over the airfoil is subdivided into a "suction flow" containing streamlines entering the airfoil suction surface, a "wake flow" containing streamlines entering the trailing-edge wake, and a "potential flow" containing all other streamlines. The suction system (fig. 2) consists of surface slots or perforations, internal airflow metering, ducting, and the compressor. The suction flow passes through the suction system and is returned to the wind-tunnel circuit far enough downstream so as not to affect the airfoil wake. An "energy defect" or decrease in total pressure occurs as a result of viscous dissipation in the sucked portion of the boundary layer and because of flow through the airfoil surface into the airfoil ducts. The portion of this energy defect that occurs upstream of the suction nozzle throat is represented as the suction drag, $c_{d,s}$. Total drag is then defined as the sum of the drag associated with the energy defect in the suction system and the wake drag associated with momentum defect in the wake:

$$c_{d,\text{total}} = c_{d,s} + c_{d,W}$$

Suction Drag Coefficient

The expression for the suction drag coefficient derived below is that used throughout the LFC tests in the 8-ft TPT. It is important to emphasize that this suction drag represents the energy deficit due to moving air through the airfoil surface and internal airfoil ducting as far as the throat of the suction nozzle (fig. 2(c)) and then returning this air to

free-stream temperature and pressure. No attempt is made to evaluate energy losses in the connector hoses, suction controls, or compressor.

Derivation. The net power delivered to the suction flow, L_s, is defined as the product of the free-stream velocity and an equivalent suction drag:

$$L_s = D_s U_\infty$$

The suction drag coefficient is then

$$\begin{aligned} c_{d,s} &= \frac{D_s}{q_\infty S} = \frac{D_s}{0.5\rho_\infty U_\infty^2 S} = \frac{2D_s}{\rho_\infty U_\infty^2 S} \\ &= \frac{2D_s U_\infty}{\rho_\infty U_\infty^3 S} = \frac{2L_s}{\rho_\infty U_\infty^3 S} \end{aligned} \tag{1}$$

Note that this equation applies to one surface (area = S) of the airfoil. The suction power L_s equals the energy defect per unit time resulting from the flow through the internal airfoil airflow ducting system. The suction power $L_s = c_p \dot{m} \Delta T_{t,sc}$ (where c_p is the specific heat at constant pressure) has previously been defined in reference 14 (ch. 5, eq. (5.7)). Therefore, since $\dot{m} = \frac{dm}{dt} = [-\rho w S]_{ws}$, where the negative sign arises from the definition of z, the local surface normal coordinate, as positive out from the surface

$$L_s = \int_{\text{L.E.}}^{\text{T.E.}} \Delta T_{t,sc} c_p S[-(\rho w)_{ws}]\, d\left(\frac{s}{c}\right) = D_s U_\infty \tag{2}$$

or

$$L_s = \int_{\text{L.E.}}^{\text{T.E.}} \Delta T_{t,sc} c_p S \rho_\infty u_\infty [-(\rho w)_{ws}/\rho_\infty u_\infty]\, d\left(\frac{s}{c}\right) \tag{3}$$

Now, by substitution of equation (3) into equation (1) the suction drag coefficient may be expressed as

$$c_{d,s} = \frac{2\int_{\text{L.E.}}^{\text{T.E.}} \Delta T_{t,sc} c_p S \rho_\infty u_\infty [-(\rho w)_{ws}/\rho_\infty u_\infty]\, d\left(\frac{s}{c}\right)}{\rho_\infty U_\infty^3 S} \tag{4a}$$

or

$$c_{d,s} = \frac{2c_p u_\infty}{U_\infty^3} \int_{\text{L.E.}}^{\text{T.E.}} \Delta T_{t,sc} [-(\rho w)_{ws}/\rho_\infty u_\infty]\, d\left(\frac{s}{c}\right) \tag{4b}$$

The term $\Delta T_{t,sc}$ is the temperature increase involved in returning air in the suction duct to free-stream pressure and velocity.

$$\Delta T_{t,sc} = \Delta T_{\text{compression}} + \Delta T_{\text{acceleration}} \tag{5}$$

The temperature increase involved in compressing the air from suction duct pressure p_{sc} to free-stream pressure p_∞ is given (in the isentropic perfect gas approximation) by

$$\Delta T_{\text{compression}} = T_{t,sc}\left[\left(\frac{p_\infty}{p_{sc}}\right)^{\frac{\gamma-1}{\gamma}} - 1\right] \tag{6}$$

In addition to being compressed to free-stream pressure p_∞, the air (essentially at rest in the duct) must be accelerated to free-stream velocity, U_∞. Using the adiabatic energy equation, this further temperature increase is

$$\Delta T_{\text{acceleration}} = \frac{\gamma - 1}{2} M_\infty^2 T_\infty \tag{7}$$

Upon substitution of equations (6) and (7) into equation (5)

$$\begin{aligned} \Delta T_{t,sc} = {} & \frac{\gamma - 1}{2} M_\infty^2 T_\infty \\ & + T_{t,sc}\left[\left(\frac{p_\infty}{p_{sc}}\right)^{\frac{\gamma-1}{\gamma}} - 1\right] \end{aligned} \tag{8}$$

Substitution of equation (8) into equation (4b) for the suction drag gives

$$\begin{aligned} c_{d,s} = {} & \frac{2c_p u_\infty}{U_\infty^3} \int_{\text{L.E.}}^{\text{T.E.}} \left[\frac{-(\rho w)_{ws}}{\rho_\infty u_\infty}\right] \\ & \times \left\{ \frac{\gamma - 1}{2} M_\infty^2 T_\infty \right. \\ & \left. + T_{t,sc}\left[\left(\frac{p_\infty}{p_{sc}}\right)^{\frac{\gamma-1}{\gamma}} - 1\right] \right\} d\left(\frac{s}{c}\right) \end{aligned} \tag{9}$$

It can be shown that since, in the standard perfect gas approximation, the free-stream speed of sound $a_\infty = \sqrt{\gamma R T_\infty}$, and $\gamma = c_p/c_v$, $R = c_p - c_v$, and $M_\infty = U_\infty/a_\infty$

$$U_\infty^2 = 2c_p \frac{\gamma - 1}{2} M_\infty^2 T_\infty \tag{10}$$

Thus with $u_\infty = U_\infty \cos\Lambda$ we can substitute equation (10) into equation (9) and write the term outside the integral in equation (9) as

$$\begin{aligned} \frac{2c_p u_\infty}{U_\infty^3} &= \frac{2c_p U_\infty \cos\Lambda}{2c_p U_\infty \frac{\gamma-1}{2} M_\infty^2 T_\infty} \\ &= \frac{2\cos\Lambda}{M_\infty^2(\gamma - 1)T_\infty} \end{aligned} \tag{11}$$

Equation (9) becomes, therefore,

$$c_{d,s} = \frac{2\cos\Lambda}{M_\infty^2(\gamma-1)T_\infty}\int_{\text{L.E.}}^{\text{T.E.}}\left[\frac{-(\rho w)_{ws}}{\rho_\infty u_\infty}\right] \times\left\{\frac{\gamma-1}{2}M_\infty^2 T_\infty + T_{t,sc} \times\left[\left(\frac{p_\infty}{p_{sc}}\right)^{\frac{\gamma-1}{\gamma}}-1\right]\right\} d\left(\frac{s}{c}\right) \quad (12)$$

or, finally, the equation used to evaluate the suction drag coefficient from experimental data

$$c_{d,s} = \frac{\cos\Lambda}{0.2M_\infty^2}\int_{\text{L.E.}}^{\text{T.E.}} C_{Q,sc} \times\left\{0.2M_\infty^2 + \frac{T_{t,sc}}{T_\infty}\left[\left(\frac{p_\infty}{p_{sc}}\right)^{\frac{\gamma-1}{\gamma}}-1\right]\right\} d\left(\frac{s}{c}\right) \quad (13)$$

where $C_{Q,sc} = \left[\frac{-(\rho w)_{ws}}{\rho_\infty u_\infty}\right]$. The evaluation of the term

$$C_{Q,sc} = \left[\frac{-(\rho w)_{ws}}{\rho_\infty u_\infty}\right]$$

from experimentally measured quantities is presented in the appendix. Note that, for values of s/c where there is no suction, $C_{Q,sc}$ is zero and so the integrand in equation (13) is also zero.

Equation (13) allows the evaluation of the equivalent suction drag coefficient for one surface of the LFC airfoil due to the energy deficit associated with returning suction duct air to free-stream conditions. Although the energy lost in forcing air through the skin slots or perforations is accounted for, the energy dissipated in the wall boundary layer of the suction hoses downstream of the nozzle and the efficiency of the suction compressor are not represented in any way in this equation.

Note that what is computed in equation (13) is a section drag coefficient, since the integration is carried out only in the stream direction, and the flow through the surface takes place over an area (chord × unit span) of model surface. As the wake drag coefficient computed from a wake rake is also a section drag coefficient, the drag represented by equation (13) is the appropriate suction drag to add to the wake drag to obtain the total drag of the suction airfoil for comparison with the drag of nonsuction airfoils.

Sample computation. As an example of the use of equation (13) in the data reduction process for the slotted airfoil used in the LFC experiment, the terms of the equation are computed for duct 9 (a typical duct in the center of the upper surface) for a typical case at design Reynolds number ($R_c = 20 \times 10^6$). Taking the terms in order from left to right

$\Lambda = 23°$
$M_\infty = 0.8188$
$T_{t,\infty} = 547.54°\text{R}$
$p_\infty = 937.3$ psf

and thus (from the standard adiabatic perfect gas equation for M_∞ and $T_{t,\infty}$), $T_\infty = 482.80°\text{R}$.

The limits of integration are, for this example, the upstream and downstream boundaries of the duct: $\Delta(s/c) = (30.969 \text{ in.} - 25.571 \text{ in.})/78.096 \text{ in.} = 0.06912$ and the quantities in the terms under the integral are assumed constant over the chordwise extent of the duct.

For measured values of nozzle throat drop $\Delta p_N = -29.28$ psf, duct temperature $T_{t,sc} = 532.17°\text{R}$, and duct static pressure $p_{sc} = 433.98$ psf, $C_{Q,sc}$ for duct 9 may be calculated from equation (A3) of the appendix to be

$$C_{Q,sc} = \left[\frac{-(\rho w)_{ws}}{\rho_\infty U_\infty}\right] = 0.000122285$$

With $\gamma = 1.4$, we may now compute (from eq. (13)) that the contribution of duct 9 to the suction drag coefficient is 0.00002555. Although equation (13) is derived as an integral, in actual use it is a discrete summation, and this suction drag coefficient computed for duct 9 is the 9th term of the summation. There would be 24 parallel terms for the slotted airfoil upper surface (21 terms for the perforated) and another 21 terms for the lower surface.

It should be noted that the numbers in this example are given to greater precision than is actually available from the instrumentation. In general, pressure errors are at least on the order of 1 psf (except for the instruments used to measure tunnel total and static pressures, which are accurate to 0.2 psf, giving a Mach number precision of 0.0007) and temperature errors at least 1°R. Based on these estimates, the number computed as $C_{Q,sc}$ of duct 9 (0.000122285) has a possible error of ±0.000002 ($C_{Q,sc} = 0.000120$ to 0.000124), and the computed suction drag coefficient has a possible error of ±0.000001 (duct 9 $\Delta c_{d,s} = 0.000025$ to 0.000026).

Wake Drag Coefficient

Five expressions for the wake drag of a swept 2-D airfoil are derived, three based on theoretical boundary-layer parameters that would be difficult to measure experimentally, and two based on wake-rake data that do not fully account for the cross-flow effect induced by the airfoil sweep. Note that the three

methods (the "leading-edge-perpendicular" method, the "streamwise" method, and the "semiempirical" method) based on theoretical boundary-layer parameters assume that these boundary-layer parameters can be carried across the trailing edge singularity into the wake.

Baals and Mourhess method. The wake drag of the airfoil in the LFC wind-tunnel experiment (ref. 7) is evaluated by the conventional momentum deficit method of reference 2. This is the method that is commonly used for the computation of the wake drag of unswept airfoils. The design calculations for the slotted LFC airfoil in the 8-ft TPT (ref. 15) indicated that the wake outer edge cross-flow angles at the wake rake are within the angle range for total pressure measurement error less than 1 percent, that is, $\pm 20°$ with respect to the wake-rake total tube plane. The wake rake is located 8 in. or 9.4 percent chord downstream of the airfoil trailing edge and aligned, in the airfoil-chord plane, parallel to the tunnel reference centerline. The rake face is aligned (in the downflow plane) perpendicular to the camberline tangent plane through the trailing edge of the airfoil with 0° flap deflection. (See figs. 4 and 5.)

Flow visualization data, using tufts on the rake, indicate that, while the extreme end of the rake above the airfoil upper surface is aligned with the flow and the extreme end of the rake below the airfoil lower surface is at about −10° yaw (that is, in the airfoil chord plane) to the flow, the center of the rake may be inclined as much as +30° yaw to the flow. This will result in a computed wake drag that is 5 to 10 percent high (1/2 to 1 count of drag at design Mach number and chord Reynolds number of 10×10^6) based on the total-tube angle error and wake drag calculations of references 16 and 17. These results indicate that it would have been extremely difficult to devise a better wake rake, since the local spanwise flow angle seems to vary by 40° over the thickness of the wake at this position downstream of the swept airfoil.

Leading-edge-perpendicular method. Realizing the limitations involved in application of the standard 2-D wake drag computation to a swept airfoil, we will present here an analysis that will give some indication of the relative magnitude of the cross-flow effect on the wake drag.

Applying the approach used by Raetz (appendix I of ref. 5), we may begin with the following expression for the wake drag of an untapered swept airfoil. The wake drag is defined as the momentum loss of the external airflow far downstream of the trailing edge where the static pressure equals the free-stream value:

$$c_{d,W} = \frac{2D_W}{\rho_\infty U_\infty^2 S} \tag{14a}$$

or, in terms of the wake momentum thickness (see ref. 1),

$$c_{d,W} = \frac{2\theta}{c} \tag{14b}$$

Now consider a spanwise segment of the airfoil, dy, with chord c_N. The velocity deficit for this segment is determined far downstream of the trailing edge so that the static-pressure field everywhere in the wake is essentially equal to free-stream static pressure. Considering the sketch in figure 4, an expression for the compressible flow per unit time of the momentum component in the streamwise direction, $\rho U = \rho(u \cos \Lambda + v \sin \Lambda)$, (through a unit area face of control volume just downstream of and parallel to the trailing edge) is

$$I_{\text{downstream}} = \rho(u \cos \Lambda + v \sin \Lambda) u \, dy \, dz \tag{15}$$

and the momentum flow

$$\rho_\infty U_\infty = \rho_\infty (u_\infty \cos \Lambda + v_\infty \sin \Lambda)$$

in through the upstream face of the same control volume is

$$I_{\text{upstream}} = \rho_\infty (u_\infty \cos \Lambda + v_\infty \sin \Lambda) u_\infty \, dy \, dz \tag{16}$$

Thus, the integral of the difference between expressions (16) and (15) over the upstream and downstream faces of the control volume equals the net flow per unit time into the control volume of the momentum component in the streamwise direction, which is the drag:

$$D_W = \int_{-\infty}^{\infty} \int_{-\infty}^{\infty} (I_{\text{upstream}} - I_{\text{downstream}})$$

With conservation of mass in the control volume,

$$\dot{m}_{\text{control volume}} = \int_{-\infty}^{\infty} \int_{-\infty}^{\infty} (\rho u - \rho_\infty u_\infty) \, dy \, dz = 0$$

Thus $\dot{m}_{\text{control volume}} u_\infty \cos \Lambda = 0$ and $\dot{m}_{\text{control volume}} v_\infty \sin \Lambda = 0$. Taking the sum of these zero terms with the difference of expressions (16) and (15)

$$D_W = \int_{-\infty}^{\infty} \int_{-\infty}^{\infty} (I_{\text{upstream}} - I_{\text{downstream}}) + \dot{m}_{\text{control volume}} u_\infty \cos \Lambda + \dot{m}_{\text{control volume}} v_\infty \sin \Lambda$$

and rearranging the terms, the drag can be expressed

$$D_W = \int_{-\infty}^{\infty}\int_{-\infty}^{\infty} \rho u\Big[(u_\infty - u)\cos\Lambda + (v_\infty - v)\sin\Lambda\Big]\,dy\,dz$$

Since all variables are assumed constant along sweep lines, $\int dy = b_N$ and, because we want to compute a section drag, $b_N = 1$ and so

$$D_W = \int_{-\infty}^{\infty} \rho u\big[(u_\infty - u)\cos\Lambda + (v_\infty - v)\sin\Lambda\big]\,dz \tag{17}$$

or

$$\begin{aligned}\frac{D_W}{0.5\rho_\infty U_\infty^2 c\cos\Lambda} &= \frac{2}{\rho_\infty U_\infty^2 c}\int_{-\infty}^{\infty}\rho u\Big[(u_\infty - u) + (v_\infty - v)\tan\Lambda\Big]\,dz \\ &= \frac{2\rho_\infty u_\infty}{\rho_\infty U_\infty c}\left[\frac{u_\infty}{U_\infty}\int_{-\infty}^{\infty}\frac{\rho u}{\rho_\infty u_\infty}(1 - u/u_\infty)\,dz\right. \\ &\quad \left. + \frac{v_\infty\tan\Lambda}{U_\infty}\int_{-\infty}^{\infty}\frac{\rho u}{\rho_\infty u_\infty}(1 - v/v_\infty)\,dz\right]\end{aligned}$$

For $S = bc$, the wake drag coefficient (eq. (14a)) may be expressed as

$$c_{d,W} = \frac{2D_W}{\rho_\infty U_\infty^2 bc} \tag{18a}$$

and so

$$\begin{aligned}\frac{c_{d,W}}{\cos\Lambda} = \frac{2\rho_\infty u_\infty}{\rho_\infty U_\infty c}\left[\frac{u_\infty}{U_\infty}\int_{-\infty}^{\infty}\frac{\rho u}{\rho_\infty u_\infty}(1 - u/u_\infty)\,dz\right. \\ + \frac{v_\infty\tan\Lambda}{U_\infty}\int_{-\infty}^{\infty}\frac{\rho u}{\rho_\infty u_\infty} \\ \left.\times\,(1 - v/v_\infty)\,dz\right]\end{aligned} \tag{18b}$$

The components of the momentum thickness

$$\theta_{uu} = \int_{-\infty}^{\infty}\frac{\rho u}{\rho_e u_e}\left(1 - \frac{u}{u_e}\right)dz$$

and

$$\theta_{vu} = \int_{-\infty}^{\infty}\frac{\rho u}{\rho_e u_e}\left(1 - \frac{v}{v_e}\right)dz$$

are

$$\left.\begin{aligned}(\theta_{uu})_\infty &= \int_{-\infty}^{\infty}\frac{\rho u}{\rho_\infty u_\infty}\left(1 - \frac{u}{u_\infty}\right)dz \\ (\theta_{vu})_\infty &= \int_{-\infty}^{\infty}\frac{\rho u}{\rho_\infty u_\infty}\left(1 - \frac{v}{v_\infty}\right)dz\end{aligned}\right\} \tag{19a}$$

far downstream of the trailing edge. Equation (18b) may be expressed as

$$\begin{aligned}\frac{c_{d,W}}{\cos\Lambda} = \frac{2u_\infty}{U_\infty}\left[\frac{u_\infty(\theta_{uu})_\infty}{U_\infty c}\right. \\ \left. + \frac{v_\infty}{U_\infty}\frac{(\theta_{vu})_\infty}{c}\tan\Lambda\right]\end{aligned} \tag{19b}$$

Letting $u_\infty = U_\infty\cos\Lambda$ and $v_\infty = U_\infty\sin\Lambda$, substitution of equations (19a) into (19b) gives

$$\begin{aligned}\frac{c_{d,W}}{\cos\Lambda} = 2\left[\frac{(\theta_{uu})_\infty}{c}\cos^2\Lambda\right. \\ \left. + \frac{(\theta_{vu})_\infty}{c}\sin\Lambda\cos\Lambda\tan\Lambda\right]\end{aligned}$$

or

$$\begin{aligned}c_{d,W} = 2\cos\Lambda\left[\frac{(\theta_{uu})_\infty}{c}\cos^2\Lambda\right. \\ \left. + \frac{(\theta_{vu})_\infty}{c}\sin^2\Lambda\right]\end{aligned} \tag{20}$$

which is the wake drag coefficient for a constant-chord swept airfoil according to Raetz (appendix I of ref. 5). In essence, Λ represents the sweep angle of the isobars and is used to determine the direction of the component of velocity that is modified by the pressure gradients downstream of the airfoil trailing edge.

The momentum thickness terms in equation (20), $(\theta_{uu})_\infty$ and $(\theta_{vu})_\infty$, are momentum deficits far downstream of the airfoil in the direction perpendicular to the leading edge. To evaluate $(\theta_{uu})_\infty$ and $(\theta_{vu})_\infty$ in terms of quantities at the airfoil trailing edge, one must consider the momentum thickness of the wake at the trailing edge with cross-flow effects due to sweep. Again following the approach used by Raetz (appendix I of ref. 5), and by Squire and Young (ref. 1), for the momentum integral equations downstream of the trailing edge (x- and z-directions with v constant) and assuming that the shearing stress is

zero,

$$\frac{d\theta_{uu}}{dx} + (H+2)\frac{\theta_{uu}}{u_e}\frac{du_e}{dx} = 0 \qquad (21a)$$

where $H = \delta^*/\theta$. Because the net transport of spanwise momentum into a control volume aligned perpendicular to the trailing edge must be zero from the assumption that all parameters are invariant along sweep lines,

$$\frac{d}{dx}(u_e\theta_{vu}) = 0$$

and, therefore,

$$u_e\theta_{vu} = \text{Constant} \qquad (21b)$$

where x is the perpendicular distance from the trailing edge and u_e is the velocity (perpendicular to the trailing edge) at the edge of the wake. Equation (21a) may then be written (dividing by θ_{uu})

$$\frac{1}{\theta_{uu}}\frac{d\theta_{uu}}{dx} = -(H+2)\frac{d}{dx}\left(\ln\frac{u_e}{u_\infty}\right) \qquad (22)$$

Integrating equation (22) over the distance x from the trailing edge to a point sufficiently downstream such that $u = u_\infty$ and $p = p_\infty$

$$\left|\ln\theta_{uu}\right|_\infty^{\text{T.E.}} = -\left|(H+2)\ln\frac{u_e}{u_\infty}\right|_\infty^{\text{T.E.}} + \int_\infty^{\text{T.E.}} \ln\frac{u_e}{u_\infty}\frac{dH}{dx}\,dx \qquad (23)$$

For large distances downstream of the trailing edge, $H = 1$ at $x = \infty$, so

$$\ln\frac{(\theta_{uu})_{\text{T.E.}}}{(\theta_{uu})_\infty} + (H_{\text{T.E.}}+2)\ln\frac{u_{e,\text{T.E.}}}{u_\infty} = \int_{H=1}^{\text{T.E.}} \ln\frac{u_e}{u_\infty}\,dH \qquad (24)$$

$H_{\text{T.E.}}$ is the value of the shape factor at the trailing edge and may be obtained from boundary-layer calculations. Then in terms of the integral in equation (24) and $u_{e,\text{T.E.}}$

$$\frac{(\theta_{uu})_\infty}{(\theta_{uu})_{\text{T.E.}}} = \left(\frac{u_{e,\text{T.E.}}}{u_\infty}\right)^{H_{\text{T.E.}}+2} e^{\int_1^{\text{T.E.}} \ln\frac{u_\infty}{u_e}\,dH} \qquad (25)$$

Evaluation of the integral in equation (25) requires a relationship between the static pressure in the wake (determines the value of u_e) and the velocity distribution in the wake (determines the value of H). Both $\ln(u_\infty/u_e)$ and H simultaneously decrease monotonically along the wake from the trailing edge to a large distance downstream, i.e.,

$$\ln(u_\infty/u_e) = 0 \text{ (far downstream, where } H = 1)$$

If we assume, as in reference 5, that

$$\frac{\ln(u_\infty/u_e)}{H-1} = \text{Constant}$$

then the integral in equation (25) can be written

$$\int_1^{\text{T.E.}} \ln\left(\frac{u_\infty}{u_e}\right)dH = \frac{H_{\text{T.E.}}-1}{2}\ln\left(\frac{u_\infty}{u_{e,\text{T.E.}}}\right) \qquad (26)$$

Substitution of equation (26) into equation (25) gives

$$\frac{(\theta_{uu})_\infty}{(\theta_{uu})_{\text{T.E.}}} = \left(\frac{u_{e,\text{T.E.}}}{u_\infty}\right)^{H_{\text{T.E.}}+2} e^{\frac{H_{\text{T.E.}}-1}{2}\ln\left(\frac{u_\infty}{u_{e,\text{T.E.}}}\right)} = \left(\frac{u_{e,\text{T.E.}}}{u_\infty}\right)^{H_{\text{T.E.}}+2}\left(\frac{u_\infty}{u_{e,\text{T.E.}}}\right)^{\frac{H_{\text{T.E.}}-1}{2}}$$

or

$$\frac{(\theta_{uu})_\infty}{(\theta_{uu})_{\text{T.E.}}} = \left(\frac{u_{e,\text{T.E.}}}{u_\infty}\right)^{\frac{H_{\text{T.E.}}+5}{2}} \qquad (27)$$

Furthermore, from equation (21b), $\frac{d}{dx}(u_e\theta_{vu}) = 0$, and so we can integrate exactly to get

$$\frac{(\theta_{vu})_\infty}{(\theta_{vu})_{\text{T.E.}}} = \frac{u_{e,\text{T.E.}}}{u_\infty} \qquad (28)$$

Then, by substituting equations (27) and (28) into equation (20), we get the expression for the coefficient of wake drag

$$c_{d,W} = \frac{2\cos\Lambda}{c}\left[(\theta_{uu})_{\text{T.E.}}\left(\frac{u_{e,\text{T.E.}}}{u_\infty}\right)^{\frac{H_{\text{T.E.}}+5}{2}}\cos^2\Lambda + (\theta_{vu})_{\text{T.E.}}\left(\frac{u_{e,\text{T.E.}}}{u_\infty}\right)\sin^2\Lambda\right] \qquad (29)$$

Equation (29) allows the computation of a wake drag that can be added to the suction drag of equation (13) to yield the total drag of the LFC airfoil:

$$c_{d,\text{total}} = c_{d,s} + c_{d,W} \qquad (30)$$

To illustrate the use of equation (29), theoretical values of the boundary-layer momentum thicknesses and edge velocities computed for the LFC airfoil at design conditions (taken from unpublished results based on the methods of ref. 11) presented in table II(a) are used to calculate $c_{d,W}$, and the results

are given in table II(b). Note that the boundary-layer parameters θ and δ^* based on flow perpendicular (uu) and parallel (vu) to the leading edge of the swept airfoil are of roughly the same order of magnitude and that the second term in equation (29) is as large as 22 percent of the first term. In the original theoretical calculations for the design of the LFC airfoil, the onset flow was broken down into orthogonal components perpendicular and parallel to the airfoil, so that equation (29) is the appropriate computation of the drag from the theoretical boundary layer. This equation has not been used for the experimental drag coefficient, however, because of the difficulty in measuring velocity components u and v.

Streamwise method. The computation represented by equation (29) can be carried out with theoretical values of θ_{uu} and θ_{vu} obtained from a boundary-layer calculation in a plane perpendicular to the airfoil leading edge. However, such boundary-layer values cannot be measured experimentally.

In an effort to evaluate the cross-flow effect on wake drag from quantities in the streamwise direction, which could be measured experimentally, the following approach due to Groth (ref. 3) was used. New coordinates in the directions parallel and perpendicular to the free-stream flow are defined and the local boundary-layer velocity coordinates u and v transformed into u_p and v_p as follows. (See fig. 4.)

$$\left.\begin{aligned} u_p &= \frac{u_e}{U_e}u + \frac{v_e}{U_e}v \\ v_p &= -\frac{v_e}{U_e}u + \frac{u_e}{U_e}v \end{aligned}\right\} \tag{31}$$

Note that this analysis applies to only one side of the airfoil at a time.

The boundary-layer displacement and momentum thicknesses are defined in the new coordinate system as follows:

$$\left.\begin{aligned} \delta^*_{u_p} &= \int_0^\infty \left(1 - \frac{\rho u_p}{\rho_\infty U_e}\right) dz \\ \delta^*_{v_p} &= \int_0^\infty \frac{\rho v_p}{\rho_\infty U_e}\, dz \\ \theta_{u_pu_p} &= \int_0^\infty \frac{\rho u_p}{\rho_\infty U_e}\left(1 - \frac{u_p}{U_e}\right) dz \\ \theta_{v_pu_p} &= \int_0^\infty \frac{\rho v_p u_p}{\rho_\infty U_e^2}\, dz \\ \theta_{v_pv_p} &= \int_0^\infty \frac{\rho v_p^2}{\rho_\infty U_e^2}\, dz \end{aligned}\right\} \tag{32}$$

so that

$$\theta_{uu} = \theta_{u_pu_p} + \frac{v_e}{u_e}\left(\theta_{v_pu_p} - \delta^*_{v_p}\right) + \frac{v_e}{u_e}\left(\theta_{v_pu_p} - \frac{v_e}{u_e}\theta_{v_pv_p}\right) \tag{33}$$

and

$$\theta_{vu} = \theta_{u_pu_p} + \frac{v_e}{u_e}\left(\theta_{v_pu_p} - \delta^*_{v_p}\right) - \frac{u_e}{v_e}\left(\theta_{v_pu_p} - \frac{v_e}{u_e}\theta_{v_pv_p}\right) \tag{34}$$

Or, dividing equations (33) and (34) by $\theta_{u_pu_p}$,

$$\frac{\theta_{uu}}{\theta_{u_pu_p}} = 1 + \frac{v_e}{u_e}\left(\frac{\theta_{v_pu_p} - \delta^*_{v_p}}{\theta_{u_pu_p}}\right) + \frac{v_e}{u_e}\left(\frac{\theta_{v_pu_p} - \frac{v_e}{u_e}\theta_{v_pv_p}}{\theta_{u_pu_p}}\right) \tag{35a}$$

$$\frac{\theta_{vu}}{\theta_{u_pu_p}} = 1 + \frac{v_e}{u_e}\left(\frac{\theta_{v_pu_p} - \delta^*_{v_p}}{\theta_{u_pu_p}}\right) - \frac{u_e}{v_e}\left(\frac{\theta_{v_pu_p} - \frac{v_e}{u_e}\theta_{v_pv_p}}{\theta_{u_pu_p}}\right) \tag{35b}$$

Thus, after substitution of equations (35a) and (35b), the bracketed terms in equation (29) may be expressed as

$$\begin{aligned} &(\theta_{uu})_{\text{T.E.}}\left(\frac{u_{e,\text{T.E.}}}{u_\infty}\right)^{\frac{H_{\text{T.E.}}+5}{2}}\cos^2\Lambda \\ &\quad + (\theta_{vu})_{\text{T.E.}}\left(\frac{u_{e,\text{T.E.}}}{u_\infty}\right)\sin^2\Lambda \\ &= \left[\theta_{u_pu_p} + \left(\frac{v_e}{u_e}\right)\left(\theta_{v_pu_p} - \delta^*_{v_p}\right)\right] \\ &\quad \times \left[\left(\frac{u_e}{u_\infty}\right)^{\frac{H+5}{2}}\cos^2\Lambda + \left(\frac{u_e}{u_\infty}\right)\sin^2\Lambda\right] \\ &\quad + \left[\theta_{v_pu_p} - \frac{v_e}{ue}\theta_{v_pv_p}\right]\left[\frac{v_e}{u_e}\left(\frac{u_e}{u_\infty}\right)^{\frac{H+5}{2}}\cos^2\Lambda \right. \\ &\quad \left. - \left(\frac{u_e}{u_\infty}\right)\left(\frac{u_e}{v_e}\right)\sin^2\Lambda\right] \end{aligned} \tag{36}$$

where all the terms on the right-hand side of the equation are evaluated at the trailing edge (T.E.).

If we now assume (see fig. 4) that the velocity along the sweep line at the edge of the boundary layer at the trailing edge, $(v_e)_{\text{T.E.}}$, can be taken as equal to the component of free-stream velocity in this

direction, v_∞, then

$$\left(\frac{v_e}{u_e}\right)_{\text{T.E.}} = \frac{v_\infty}{u_{e,\text{T.E.}}} = \frac{u_\infty \tan\Lambda}{u_{e,\text{T.E.}}}$$

and so the right side of equation (36) can be written

$$\begin{aligned}
&\left[\theta_{u_pu_p} + \left(\frac{u_\infty}{u_e}\right)\left(\theta_{v_pu_p} - \delta^*_{v_p}\right)\tan\Lambda\right] \\
&\quad\times\left[\left(\frac{u_e}{u_\infty}\right)^{\frac{H+5}{2}}\cos^2\Lambda + \left(\frac{u_e}{u_\infty}\right)\sin^2\Lambda\right] \\
&\quad+\left[\theta_{v_pu_p} - \frac{u_\infty}{u_e}\theta_{v_pv_p}\tan\Lambda\right] \\
&\quad\times\left[\left(\frac{u_e}{u_\infty}\right)^{\frac{H+3}{2}}\sin\Lambda\cos\Lambda\right. \\
&\quad\left.-\left(\frac{u_e}{u_\infty}\right)^{2}\sin\Lambda\cos\Lambda\right]
\end{aligned}$$

or

$$\begin{aligned}
&\theta_{u_pu_p}\left(\frac{u_\infty}{u_e}\right)^{\frac{H+5}{2}}\cos^2\Lambda \\
&\quad+\left[\left(2\theta_{v_pu_p} - \delta^*_{v_p}\right)\tan\Lambda\right]\left(\frac{u_e}{u_\infty}\right)^{\frac{H+3}{2}}\cos^2\Lambda \\
&\quad-\theta_{v_pv_p}\left(\frac{u_e}{u_\infty}\right)^{\frac{H+1}{2}}\sin^2\Lambda \\
&\quad-\theta_{v_pu_p}\left(\frac{u_e}{u_\infty}\right)^{2}\sin\Lambda\cos\Lambda \\
&\quad+\left(\theta_{u_pu_p} + \theta_{v_pv_p}\right)\left(\frac{u_e}{u_\infty}\right)\sin^2\Lambda \\
&\quad+\left(\theta_{v_pu_p} - \delta^*_{v_p}\right)\tan\Lambda\sin^2\Lambda
\end{aligned}$$

We can now substitute these expressions into equation (29) to obtain (arranged as terms in $\theta_{u_pu_p}$, $\theta_{v_pu_p}$, $\delta^*_{v_p}$, and $\theta_{v_pv_p}$)

$$\begin{aligned}
c_{d,W} = \frac{2\cos\Lambda}{c}\Bigg\{&\theta_{u_pu_p}\left[\left(\frac{u_e}{u_\infty}\right)^{\frac{H+5}{2}}\cos^2\Lambda\right. \\
&\left.+\left(\frac{u_e}{u_\infty}\right)\sin^2\Lambda\right] \\
&+\theta_{v_pu_p}\left[\left(\frac{u_e}{u_\infty}\right)^{\frac{H+3}{2}}2\tan\Lambda\cos^2\Lambda\right. \\
&\left.-\left(\frac{u_e}{u_\infty}\right)^{2}\sin\Lambda\cos\Lambda + \tan\Lambda\sin^2\Lambda\right] \\
&-\delta^*_{v_p}\left[\left(\frac{u_e}{u_\infty}\right)^{\frac{H+3}{2}}\cos^2\Lambda + \sin^2\Lambda\right]\tan\Lambda \\
&-\theta_{v_pv_p}\left[\left(\frac{u_e}{u_\infty}\right)^{\frac{H+1}{2}} - \frac{u_e}{u_\infty}\right]\sin^2\Lambda\Bigg\} \qquad (37)
\end{aligned}$$

The boundary-layer parameter components (terms in θ and δ^*) of the wake drag in this form may now be evaluated with theoretical values from unpublished results using the methods of reference 12 as presented in table III(a). These are the same basic theoretical values as were used in the leading-edge-perpendicular method, transformed into the streamwise coordinate system. It can now be seen in table III(b) that in the streamwise analysis, the contribution of spanwise terms at the airfoil trailing edge may be considered small, as the largest cross-flow term (the third term in eq. (37), a multiple of $\delta^*_{v_p}$) is 0.2 percent of the first term.

Semiempirical approximation. In the semiempirical approach for swept wings of reference 1, the wake drag coefficient is expressed in terms of variables at any point x downstream of the trailing edge as

$$c_{d,W} = \frac{2\theta_x}{c}\left(\frac{U_x}{U_\infty}\right)^{\frac{H_x+5}{2}}$$

Taking this point x as the position of a wake rake, we may write

$$c_{d,W} = \frac{2\theta_W}{c}\left(\frac{U_{e,W}}{U_\infty}\right)^{\frac{H_W+5}{2}} \qquad (38)$$

The momentum and displacement thicknesses as a function of the ratio of the measured resultant velocity in the wake to that in the free stream may be determined from the expressions

$$\left.\begin{aligned}
\theta_W &= \int_{-e}^{e}\frac{\rho U}{\rho_e U_e}\left(1 - \frac{U}{U_e}\right)dz \\
\delta^*_W &= \int_{-e}^{e}\left(1 - \frac{\rho U}{\rho_e U_e}\right)dz
\end{aligned}\right\} \qquad (39)$$

where U is the velocity determined at a wake rake oriented in the streamwise direction. The rake size and the downstream distance from the trailing edge are designed so that there is a point on each end of the rake such that $U = U_e$, beyond which the integrand is zero. Distributions of both static pressure p and total pressure p_t are measured on the rake and, using

standard compressible flow relationships,

$$U^2 = \frac{2\gamma}{\gamma - 1}\frac{p}{\rho}\left[\left(\frac{p_t}{p}\right)^{\frac{\gamma-1}{\gamma}} - 1\right] \tag{40}$$

The velocity ratio may be expressed as

$$\frac{U}{U_e} = \sqrt{\frac{p/p_e}{\rho/\rho_e}\frac{(p_t/p)^{\frac{\gamma-1}{\gamma}} - 1}{(p_{t,e}/p_e)^{\frac{\gamma-1}{\gamma}} - 1}} \tag{41}$$

where the density ratio in terms of the velocity ratio at the rake is

$$\frac{\rho}{\rho_e} = \frac{1 + \frac{\gamma-1}{2}M^2}{1 + \frac{\gamma-1}{2}M_e^2}$$

In terms of Mach number,

$$\frac{U}{U_e} = \frac{M}{M_e}\sqrt{\frac{1 + \frac{\gamma-1}{2}M_e^2}{1 + \frac{\gamma-1}{2}M^2}} \tag{42}$$

The coefficient $c_{d,W}$ of equation (38) can now be computed from pressure data measured by a rake in the airfoil wake. This has been done for the slotted airfoil data at chord Reynolds numbers of 10–15 million. A sample pressure distribution and a computed velocity distribution on the wake rake are presented in figures 6 and 7. The drag coefficients are presented in figure 8. For comparison, we also present in this figure the corresponding 2-D drag coefficient computed from the same wake-rake data by the conventional Baals and Mourhess method of reference 2.

To compare the wake drag coefficient obtained with the semiempirical approximation of equation (38) with that obtained by the leading-edge-perpendicular method of equation (29) or the streamwise method of equation (37), using the streamwise theoretical boundary-layer values of table III, assume the inviscid relationship $v_{e,\mathrm{T.E.}} = U_\infty \sin\Lambda$. Then

$$\frac{u_{e,\mathrm{T.E.}}}{u_\infty} = \frac{\sqrt{U_{\mathrm{T.E.}}^2 - (U_\infty \sin\Lambda)^2}}{U_\infty \cos\Lambda} = \left[\left(\frac{U_{\mathrm{T.E.}}}{U_\infty}\right)^2 \frac{1}{\cos^2\Lambda} - \tan^2\Lambda\right]^{1/2}$$

or

$$\frac{U_{\mathrm{T.E.}}}{U_\infty} = \left[\left(\frac{u_{e,\mathrm{T.E.}}}{u_\infty}\right)^2 + \tan^2\Lambda\right]^{1/2}\cos\Lambda \tag{43}$$

This equation provides the velocity ratio that could actually be measured by a suitable rake or survey probe at the trailing edge in terms of the perpendicular edge velocity ratio. For the purpose of comparing equations (29) and (38), equation (43) has been used to compute a streamwise velocity ratio $\frac{U_{\mathrm{T.E.}}}{U_\infty}$ from the theoretical perpendicular velocity ratio $\frac{u_{e,\mathrm{T.E.}}}{u_\infty}$ and the result is presented in table II.

The computation of wake drag from equation (38) using the theoretical boundary-layer values of table II for comparison with the value obtained from equation (29) assumes that the momentum thickness and shape factor (which are boundary-layer values) of equation (29) are adequate to this order of approximation for use in equation (38) (a wake equation). Note also that, for the purposes of this comparison, the wake drag coefficient computation from equation (38) must be carried out separately for the upper and lower surfaces.

Design streamline boundary-layer method. One further method of evaluating the theoretical wake drag of a swept untapered airfoil will be considered at this point. In the course of designing the contoured liner (ref. 15) for the test of the suction airfoil, extensive theoretical airfoil boundary-layer calculations (heretofore unpublished but used in the determination of the liner contour) were carried out along the theoretical streamlines over the airfoil surface and into the wake. (See fig. 9(a).) Assuming that, for the design case at least, the cross-flow effects are small ($v_p << u_p$), equations (33) and (34) become

$$\theta_{uu} = \theta_{u_pu_p} + \text{terms } O(\theta_{v_pu_p},\ \theta_{v_pv_p},\ \delta^*_{u_p})$$
$$\theta_{vu} = \theta_{v_pu_p} + \text{terms } O(\theta_{v_pu_p},\ \theta_{v_pv_p},\ \delta^*_{v_p})$$

Then equation (37) becomes

$$c_{d,W} = \frac{2\cos\Lambda}{c}(\theta_{u_pu_p})_{\mathrm{W.R.}}\left(\frac{u_{e,\mathrm{W.R.}}}{u_\infty}\right) \times \left[\left(\frac{u_{e,\mathrm{W.R.}}}{u_\infty}\right)^{\frac{H_{\mathrm{W.R.}}+3}{2}}\cos^2\Lambda + \sin^2\Lambda\right] + \text{terms } O(\theta_{v_pu_p},\ \theta_{v_pv_p},\ \delta^*_{v_p}) \tag{44}$$

where the subscript "W.R." denotes evaluation at the wake-rake position, $X/c = 1.094$.

For this unpublished theoretical airfoil boundary-layer data computed along the streamlines, what is available from these computations is

$$\frac{U_e}{U_\infty},\ \text{where } U_e = \sqrt{u_e^2 + v_e^2} \text{ and}$$
$$v_e = v_\infty = U_\infty \sin\Lambda,\ u_\infty = U_\infty \cos\Lambda$$

Therefore

$$\frac{U_e}{U_\infty} = \sqrt{\left(\frac{u_e}{U_\infty}\right)^2 + \left(\frac{v_e}{U_\infty}\right)^2}$$
$$= \sqrt{\left(\frac{u_e}{u_\infty}\right)^2 \cos^2\Lambda + \sin^2\Lambda}$$

or

$$\left(\frac{u_e}{u_\infty}\right)_{\text{W.R.}} = \frac{1}{\cos\Lambda}\sqrt{\left(\frac{U_e}{U_\infty}\right)^2 - \sin^2\Lambda}$$

and so equation (44) becomes

$$c_{d,W} = 2\left(\frac{\theta_{u_p u_p}}{c}\right)_{\text{W.R.}} \sqrt{\left(\frac{U_e}{U_\infty}\right)^2_{\text{W.R.}} - \sin^2\Lambda} \times \left[\left(\frac{u_e}{u_\infty}\right)^{\frac{H_{\text{W.R.}}+3}{2}}_{\text{W.R.}} \cos^2\Lambda + \sin^2\Lambda\right] \quad (45)$$

The unpublished data used for equation (45), and the result of this computation, are presented in table IV for a range of boundary-layer transition locations. To compare this theoretical wake drag coefficient with that obtained experimentally, the assumed transition values of x/c were matched with those experimentally measured on the wing centerline at chord Reynolds numbers from 10 to 20 million. (See table V.) The wake drag coefficient computed at a chord Reynolds number of 20 million (the design-point Reynolds number at which the streamline boundary-layer computations were done) was scaled to lower experimental Reynolds numbers on the basis of the well-known relationship for the turbulent wake of a flat plate (ref. 18, ch. XXI).

$$c_{d,W}\sqrt[5]{R_c} = \text{Constant} \quad (46)$$

These results are tabulated in table VI. The comparison of these theoretical wake drag coefficients with a typical experimental variation of wake drag coefficient with Reynolds number on the slotted LFC model using the conventional Baals and Mourhess method is presented in figure 9(b).

Evaluation of Drag Coefficient Analyses

Suction Drag

Equation (13) was used to evaluate the suction drag on both surfaces of the swept LFC airfoil (fig. 1) over a range of chord Reynolds numbers at a constant Mach number. The integral in equation (13) was evaluated by a summation of the theoretical suction flow coefficient C_Q (fig. 3 and tables I(b) and (c)) over the airfoil for individual ducts and corresponding theoretical suction-pressure and temperature ratios to bring the exhaust suction air of the individual ducts back to free-stream velocity and pressure. Table I gives representative upper and lower surface values of the design suction coefficients for several chord Reynolds numbers and design values of pressure and temperature ratios for individual suction ducts of the slotted airfoil. Also shown in table I are the design values of the calculated coefficient of suction drag, $c_{d,s}$, for upper and lower surfaces used to obtain the design suction drag. Equation (13) was used to obtain the suction drag coefficient for all the LFC tests in the 8-ft TPT.

Wake Drag

Five approaches to the computation of the wake drag on a swept 2-D airfoil have been presented. These are briefly summarized as follows:

1. The conventional Baals and Mourhess method (ref. 2) for the calculation of the wake drag of a 2-D airfoil from static and total pressure measurements on a wake rake has been used to compute the wake drag for all of the LFC tests in the 8-ft TPT. It is not strictly correct for a swept airfoil. Estimates based on a brief tuft test indicate that sweep-induced cross flow at the wake rake is as much as 30°, and thus the wake drag from this method could be 5 to 10 percent high because of errors in total-pressure data due to misalignment between the local wake flow direction and the individual rake probes.

2. The leading-edge-perpendicular method resulting in equation (29) is based on theoretical laminar-boundary-layer parameters computed from the component of free-stream flow that is perpendicular to the airfoil leading edge. These boundary-layer parameters could not be measured experimentally with the available instrumentation. The analysis of equation (29) indicates that the cross-flow terms are too large to ignore.

3. The transformation to a coordinate system aligned with the free-stream direction results in equation (37). The cross-flow terms are less than 0.2 percent of the total drag. The significant term in equation (37), the term involving the streamwise momentum thickness $\theta_{u_p u_p}$, could be measured experimentally but no such data were obtained during these tests.

4. The semiempirical approximation of equation (38), using the same experimental wake-rake data as the conventional Baals and Mourhess method, does not account for flow misalignment error that would cause the Baals and Mourhess drag to be

high. The two methods compare quite well at the lower Reynolds numbers, but begin to diverge for Reynolds numbers greater than 11 million, principally in the lower surface contribution, probably because the lower surface boundary layer begins to separate at 85 percent chord at this Reynolds number (see ref. 8) and thus the shape factor H in equation (38) becomes invalid.

5. The design streamline boundary-layer wake drag method (eqs. (45) and (46)), which is a simplification of equation (37) by neglecting the cross-flow terms, yields values for wake drag variation with chord Reynolds number (fig. 9(b)) that compare well with the experimental values as calculated using the Baals and Mourhess method and thus tend to confirm the liner design process.

The data reduction program for the LFC tests in the 8-ft TPT uses the conventional Baals and Mourhess method for wake drag. All the error in this method results from misalignment between the wake-rake elements and the local wake flow. This error could be reduced if the rake could be placed further downstream of the airfoil trailing edge (but other design considerations made that impossible in this series of tests) or if the rake pitch could be varied at each test condition so that the true total pressure deficit was obtained on each probe.

Tables II and III show that at the lowest Reynolds number for the theoretical boundary-layer computations, $R_c = 8 \times 10^6$, the three wake drag methods (eqs. (29), (37), and (38)) using the theoretical boundary-layer characteristics yield, for full-chord laminar flow, values of $c_{d,W} = 2.5 \times 10^{-4}$, 2.6×10^{-4}, and 3.0×10^{-4}, respectively. These methods based on theoretical boundary-layer parameters agree well with each other, as did the methods based on experimental wake data. Note that equation (38) was used both ways. However, the drag coefficients based on the theoretical full-chord laminar parameters are low compared with the experimental (Baals and Mourhess method) wake-rake drag coefficient of about 8×10^{-4} measured at $R_c = 10 \times 10^6$ even though those data were obtained with laminar flow to at least $X/c = 0.95$. It should be noted, however, that the experimental determination of 95-percent-chord laminar flow on the upper surface is based on a surface-mounted turbulence detector that was not in line with the wake rake but somewhat below it, as shown in figure 5. Extensive tuft studies indicate that even when this last downstream detector location is laminar, the wing upper surface flow at the trailing edge is very nearly parallel to the trailing edge and in the downward direction, so that the flow at the wake rake is probably contaminated to some extent by flow from nonlaminar regions further up on the wing. In addition, the patterns of laminar flow shown in reference 8 indicate that the lower surface flow immediately upstream of the wake rake was laminar only to about 60 percent (the flow above the wake rake was laminar to the end of suction, 84 percent).

Concluding Remarks

The Langley Research Center has designed a swept, supercritical airfoil incorporating laminar-flow control (LFC) for testing at transonic speeds. Analytical expressions have been developed and an evaluation has been made of the drag, including suction and wake drag, by using theoretical design information and experimental data.

The analysis shows that, although the sweep-induced boundary-layer cross-flow influence on the wake drag is too large to be ignored and there is not a practical method for evaluating these cross-flow effects experimentally, the conventional unswept Baals and Mourhess method for wake drag computation used in the reduction of the experimental data yields wake drag that is at worst 10 percent too high.

NASA Langley Research Center
Hampton, VA 23665-5225
January 10, 1989

Appendix

Evaluation of Total Suction Drag Coefficient From Flow Quantity Measurements in Calibrated Suction Duct Nozzles

The suction flow coefficient C_Q of the individual suction ducts or chambers on the swept LFC airfoil may be defined as

$$C_{Q,sc} = \frac{\dot{m}_{sc,i}}{\rho_\infty u_\infty b_N c_N} \tag{A1}$$

where $\dot{m}_{sc,i}$ is the mass flow due to suction of the ith duct, which is located between successive chordwise stations s_i and s_{i+1} and has an average span b_N and chord c_N (measured parallel and perpendicular respectively to the leading edge). The duct dimensions include in every case half of the bulkhead wall thickness so that the sum of the duct areas is exactly equal to the projected airfoil surface area. Therefore, the total suction flow coefficient of the airfoil is equal to

$$(C_{Q,sc})_{\text{total}} = \sum_{i=1}^{i=K} C_{Q,sc} = \int_0^1 \left[\frac{-(\rho w)_{ws}}{\rho_\infty u_\infty}\right] d\left(\frac{X}{c}\right) \tag{A2}$$

where K is the number of suction chambers. Values of $C_{Q,sc}$ can be determined from flow quantity measurements of individual suction nozzles located in each duct (figs. 2(c) and 10). The following equation for $C_{Q,sc}$ is based on specially designed and calibrated nozzles as previously used by Pfenninger and Groth in low-drag suction airfoil flight and wind-tunnel tests (ref. 19):

$$C_{Q,sc} = \frac{\alpha_N f \sqrt{\frac{\rho_{sc}}{\rho_\infty}\frac{\Delta p_N}{q_\infty}}}{b_N c_N \cos\Lambda \sqrt{1-(f/F)^2}} \tag{A3}$$

where $\Delta p_N = p_{sc} - p_N$ is a required measurement. The term $\cos\Lambda$ in the denominator is required because $C_{Q,sc}$ is defined in equation (A1) as nondimensionalized by $u_\infty = U_\infty \cos\Lambda$, but the q_∞ that is most convenient to use in equation (A3) is the free-stream dynamic pressure $q_\infty = 0.5\rho_\infty U_\infty^2$.

A sketch of the axisymmetric suction nozzle previously used by Pfenninger and Groth (ref. 19) and considered herein is shown in figure 10. The nozzle flow coefficient α_N is a function of Reynolds number based on nozzle diameter, assuming geometrically similar nozzles, as determined by calibration. An empirical equation for the diameter of the nozzle from the beginning of the contraction to the throat is (for $0 \le x \le 2d_N$)

$$d(x) = d_N\left(1 + \frac{3}{2}\left\{\frac{4}{\pi}\arctan\left[1 - \left(\frac{x}{2d_N}\right)^n\right]\right\}^{1/n}\right) \tag{A4}$$

where d_N is the nozzle throat diameter and the exponent $n = 2.545$. This equation fits the nozzle coordinates from the entrance plane ($x = 0$) to the throat where p_N is measured ($x = 2d_N$), to within 0.01 in. for $d_N = 1$ in. In the 8-ft TPT LFC experiments, 12 sizes of this nozzle were used, with $d_N = 0.188$ to 0.875 in.

The data reduction procedure obtains the value of α_N from an empirical equation fitted to the nozzle calibration data. The fit of the empirical equation to the data is within the error band of the calibration data. The empirical equation used in the LFC data reduction is

$$\alpha_N(R_d) = 0.927 - 0.0339787 \times \left[\sqrt{1 + 4(\log_{10} R_d - 4)^2} - 1\right] + 0.075(\log_{10} R_d - 4) \tag{A5}$$

where R_d is the Reynolds number of the nozzle throat flow based on the nozzle throat diameter d_N. This equation was fitted to data in the range $10^3 \le R_d \le 10^5$.

The suction drag may finally be expressed (eq. 13)) as follows:

$$c_{d,s} = \frac{\cos\Lambda}{0.2M_\infty^2}\int_{\text{L.E.}}^{\text{T.E.}} C_{Q,sc}\left\{0.2M_\infty^2 + \frac{T_{t,sc}}{T_\infty}\left[\left(\frac{p_\infty}{p_{sc}}\right)^{\frac{\gamma-1}{\gamma}} - 1\right]\right\} d\left(\frac{s}{c}\right) \tag{A6}$$

The experimental accuracy to which the suction drag coefficient can be determined for a single duct is primarily dependent upon the accuracy to which Δp (the drop in pressure from the duct to the nozzle throat) can be measured. Inspection of equation (A3) for the suction flow coefficient reveals that $C_{Q,sc}$ is proportional to $(\Delta p_N)^{0.5}$ with all other quantities constant, except for the effect of α_N, which is a function of nozzle throat Reynolds number and is determined from calibration. Therefore, in low-drag experiments involving determination of the suction drag as part of the total drag, when equation (A6) is applied, the data accuracy required should be

analyzed and a suitable measurement technique (instrumentation) selected. Note that the sweep Λ appears in equation (A6) (and eq. (13)) because $C_{Q,sc}$ is defined in terms of the velocity $u_\infty = U_\infty \cos\Lambda$, perpendicular to the wing leading edge, while the desired suction drag coefficient $c_{d,s}$ is in the free-stream direction.

References

1. Squire, H. B.; and Young, A. D.: *The Calculation of the Profile Drag of Aerofoils.* R. & M. No. 1838, British Aeronautical Research Council, 1938.
2. Baals, Donald D.; and Mourhess, Mary J.: *Numerical Evaluation of the Wake-Survey Equations for Subsonic Flow Including the Effect of Energy Addition.* NACA WR L-5, 1945. (Formerly NACA ARR L5H27.)
3. Groth, E. E.: Low Drag Boundary Layer Suction Experiments on a 36° Swept Wing at Mach Numbers 2.5, 3.0, and 3.5. *Summary of Laminar Boundary Layer Control Research—Volume II,* ASD-TDR-63-554, U.S. Air Force, Mar. 1964, pp. 464–480. (Available from DTIC as AD 605 186.)
4. Goldsmith, J.: Low Drag Boundary Layer Suction Experiments on a 72° Swept Wing Model at Mach Numbers 2.0 and 2.25. *Summary of Laminar Boundary Layer Control Research—Volume II,* ASD-TDR-63-554, U.S. Air Force, Mar. 1964, pp. 487–508. (Available from DTIC as AD 605 186.)
5. Pfenninger, W.; Gross, Lloyd; and Bacon, John W., Jr. (appendix I by G. S. Raetz): *Experiments on a 30° Swept 12%-Thick Symmetrical Laminar Suction Wing in the 5-Ft by 7-Ft Michigan Tunnel.* Rep. No. NAI-57-317 (BLC-93), Northrop Aircraft, Inc., Feb. 1957.
6. Goldsmith, John: *A Suggested Procedure for Determining the Wake Drag of Highly Swept Wings by Means of Simple Wake Measurements.* Rep. No. NOR-65-285 (BLC-165), Northrop Corp., Oct. 1965.
7. Harris, Charles D.; Harvey, William D.; and Brooks, Cuyler W., Jr.: *The NASA Langley Laminar-Flow-Control Experiment on a Swept, Supercritical Airfoil—Design Overview.* NASA TP-2809, 1988.
8. Harris, Charles D.; Brooks, Cuyler W., Jr.; Clukey, Patricia C.; and Stack, John P.: The NASA Langley Laminar-Flow-Control Experiment on a Swept, Supercritical Airfoil—Basic Results for Slotted Configuration. NASA TM-4100, 1989.
9. Pfenninger, W.; Reed, Helen L.; and Dagenhart, J. R.: Design Considerations of Advanced Supercritical Low Drag Suction Airfoils. *Viscous Flow Drag Reduction,* Gary R. Hough, ed., American Inst. of Aeronautics and Astronautics, c.1980, pp. 249–271.
10. Maddalon, Dal V.; and Poppen, William A., Jr.: *Design and Fabrication of Large Suction Panels With Perforated Surfaces for Laminar Flow Control Testing in a Transonic Wind Tunnel.* NASA TM-89011, 1986.
11. Dagenhart, J. Ray: *Amplified Crossflow Disturbances in the Laminar Boundary Layer on Swept Wings With Suction.* NASA TP-1902, 1981.
12. El-Hady, Nabil M.: On the Stability of Three-Dimensional Compressible Nonparallel Boundary Layers. AIAA-80-1374, July 1980.
13. Mack, Leslie M.: On the Stability of the Boundary Layer on a Transonic Swept Wing. AIAA-79-0264, Jan. 1979.
14. Liepmann, H. W.; and Roshko, A.: *Elements of Gasdynamics.* John Wiley & Sons, Inc., c.1957.
15. Newman, Perry A.; Anderson, E. Clay; and Peterson, John B., Jr.: *Aerodynamic Design of the Contoured Wind-Tunnel Liner for the NASA Supercritical, Laminar-Flow-Control, Swept-Wing Experiment.* NASA TP-2335, 1984.
16. Bryer, D. W.; and Pankhurst, R. C.: *Pressure-Probe Methods for Determining Wind Speed and Flow Direction.* Her Majesty's Stationery Off. (London), 1971.
17. Gracey, William; Letko, William; and Russell, Walter R.: *Wind-Tunnel Investigation of a Number of Total-Pressure Tubes at High Angles of Attack—Subsonic Speeds.* NACA TN 2331, 1951. (Supersedes NACA RM L50G19.)
18. Schlichting, Hermann (J. Kestin, transl.): *Boundary-Layer Theory, Sixth ed.* McGraw-Hill Book Co. Inc., c.1968.
19. Pfenninger, W.; and Groth, E.: Low Drag Boundary Layer Suction Experiments in Flight on a Wing Glove of an F-94A Airplane With Suction Through a Large Number of Fine Slots. *Boundary Layer and Flow Control, Volume 2,* G. V. Lachmann, ed., Pergamon Press, 1961, pp. 981–999.

Table I. Representative Theoretical Values of the Suction Drag Coefficient and Suction-Chamber Parameters on the Upper and Lower Slotted LFC Airfoil Surfaces

$[M_\infty = 0.82,\ \Lambda = 23°]$

(a) Suction coefficient and suction drag coefficient as integrated from table I(b) parameters

R_c	C_Q	$c_{d,s}$ (eq. (13))
Upper surface		
8×10^6	3.848×10^{-4}	5.164×10^{-4}
20	2.970	4.051
40	2.464	3.408
Lower surface		
8×10^6	6.568×10^{-4}	7.054×10^{-4}
20	5.142	5.492
40	4.319	4.589

Table I. Continued

$[R_c = 20 \times 10^6]$

(b) Upper surface suction-chamber pressure and temperature ratios and suction-coefficient variation with X/c

Duct	X/c	p_{sc}/p_∞	$T_\infty/T_{t,sc}$	C_Q
	0			
	$.0434 \times 10^{-3}$			
	$.7782 \times 10^{-3}$			
	$.2064 \times 10^{-2}$			
	$.3959 \times 10^{-2}$			
	$.6613 \times 10^{-2}$			
	$.9738 \times 10^{-2}$			
	$.1369 \times 10^{-1}$			
	$.1841 \times 10^{-1}$			
	$.2389 \times 10^{-1}$			
1	$.3012 \times 10^{-1}$	0.6113	0.9570	-0.1200×10^{-3}
1	$.3709 \times 10^{-1}$	.6113	.9570	$-.1160 \times 10^{-3}$
2	$.4478 \times 10^{-1}$	.6345	.9586	$-.1130 \times 10^{-3}$
2	$.5317 \times 10^{-1}$	.6345	.9586	$-.1080 \times 10^{-3}$
2	$.6225 \times 10^{-1}$	.6345	.9586	$-.1040 \times 10^{-3}$
2	$.7201 \times 10^{-1}$	.6345	.9586	$-.1060 \times 10^{-3}$
3	$.8247 \times 10^{-1}$	.6445	.9596	$-.1040 \times 10^{-3}$
3	$.9347 \times 10^{-1}$	.6445	.9596	$-.1020 \times 10^{-3}$
3	.1051	.6445	.9596	$-.1000 \times 10^{-3}$
4	.1174	.6498	.9603	$-.9900 \times 10^{-4}$
4	.1302	.6498	.9603	$-.9800 \times 10^{-4}$
5	.1437	.6530	.9608	$-.9800 \times 10^{-4}$
5	.1576	.6530	.9608	$-.9400 \times 10^{-4}$
5	.1721	.6530	.9608	$-.9300 \times 10^{-4}$
6	.1871	.6530	.9608	$-.9300 \times 10^{-4}$
6	.2025	.6577	.9613	$-.9200 \times 10^{-4}$
7	.2184	.6577	.9613	$-.9000 \times 10^{-4}$
7	.2349	.6607	.9618	$-.8800 \times 10^{-4}$
7	.2515	.6607	.9618	$-.8600 \times 10^{-4}$
8	.2686	.6653	.9624	$-.8200 \times 10^{-4}$
8	.2860	.6653	.9624	$-.8100 \times 10^{-4}$
8	.3038	.6653	.9624	$-.8000 \times 10^{-4}$
8	.3218	.6653	.9624	$-.8000 \times 10^{-4}$
9	.3401	.6695	.9630	$-.8000 \times 10^{-4}$
9	.3587	.6695	.9630	$-.8000 \times 10^{-4}$
9	.3774	.6695	.9630	$-.8000 \times 10^{-4}$
10	.3983	.6722	.9634	$-.8000 \times 10^{-4}$
10	.4158	.6722	.9634	$-.8000 \times 10^{-4}$
10	.4346	.6722	.9634	$-.8000 \times 10^{-4}$
10	.4538	.6722	.9634	$-.8000 \times 10^{-4}$
11	.4732	.6727	.9638	$-.8000 \times 10^{-4}$
11	.4925	.6727	.9638	$-.8000 \times 10^{-4}$
11	.5118	.6727	.9638	$-.8200 \times 10^{-4}$

Table I. Continued

(b) Concluded

Duct	X/c	p_{sc}/p_∞	$T_\infty/T_{t,sc}$	C_Q
12	0.5312	0.6734	0.9640	-0.8500×10^{-4}
12	.5504	.6734	.9640	$-.9000 \times 10^{-4}$
12	.5696	.6734	.9640	$-.9300 \times 10^{-4}$
12	.5886	.6734	.9640	$-.9900 \times 10^{-4}$
13	.6075	.6739	.9642	$-.1000 \times 10^{-3}$
13	.6261	.6739	.9642	$-.1100 \times 10^{-3}$
14	.6448	.6750	.9645	$-.1200 \times 10^{-3}$
14	.6629	.6750	.9645	$-.1400 \times 10^{-3}$
14	.6806	.6750	.9645	$-.1600 \times 10^{-3}$
15	.6985	.6832	.9653	$-.1900 \times 10^{-3}$
15	.7159	.6832	.9653	$-.2200 \times 10^{-3}$
16	.7329	.6942	.9669	$-.2600 \times 10^{-3}$
17	.7495	.6992	.9700	$-.3100 \times 10^{-3}$
18	.7657	.7180	.9749	$-.3700 \times 10^{-3}$
19	.7816	.7459	.9794	$-.4300 \times 10^{-3}$
19	.7970	.7459	.9794	$-.5100 \times 10^{-3}$
20	.8119	.8026	.9830	$-.6200 \times 10^{-3}$
20	.8264	.8026	.9830	$-.7900 \times 10^{-3}$
20	.8404	.8026	.9830	$-.1100 \times 10^{-2}$
21	.8541	.8561	.9860	$-.1740 \times 10^{-2}$
21	.8673	.8561	.9860	$-.1700 \times 10^{-2}$
22	.8803	.9072	.9887	$-.1500 \times 10^{-2}$
23	.8928	.9238	.9902	$-.1320 \times 10^{-2}$
24	.9050	.9462	.9917	$-.1130 \times 10^{-2}$
24	.9167	.9462	.9917	$-.1000 \times 10^{-2}$
24	.9276	.9462	.9917	$-.9900 \times 10^{-3}$
24	.9384	.9462	.9917	$-.1020 \times 10^{-2}$
24	.9483	.9462	.9917	$-.1070 \times 10^{-2}$
24	.9576	.9462	.9917	$-.1120 \times 10^{-2}$
24	.9663	.9462	.9917	$-.1180 \times 10^{-2}$
24	.9742	.9462	.9917	$-.1300 \times 10^{-2}$
	.9815			
	.9879			
	.9936			
	.9965			
	$.1002 \times 10^{1}$			
	$.1005 \times 10^{1}$			
	$.1008 \times 10^{1}$			
	$.1009 \times 10^{1}$			
	$.1010 \times 10^{1}$			

Table I. Continued

$[R_c = 20 \times 10^6]$

(c) Lower surface suction-chamber pressure and temperature ratios and suction-coefficient variation with X/c

Duct	X/c	p_{sc}/p_∞	$T_\infty/T_{t,sc}$	C_Q
	0			
	0.1000×10^{-3}			
	$.6228 \times 10^{-3}$			
	$.2102 \times 10^{-2}$			
	$.4595 \times 10^{-2}$			
	$.8159 \times 10^{-2}$			
	$.1277 \times 10^{-1}$			
	$.1842 \times 10^{-1}$			
	$.2504 \times 10^{-1}$			
	$.3204 \times 10^{-1}$			
	$.4122 \times 10^{-1}$			
	$.5077 \times 10^{-1}$			
1	$.6128 \times 10^{-1}$	0.1143×10^1	0.9793	-0.1000×10^{-3}
2	$.7280 \times 10^{-1}$	$.1153 \times 10^1$	.9804	$-.3000 \times 10^{-3}$
2	$.7925 \times 10^{-1}$	$.1153 \times 10^1$	.9804	$-.4000 \times 10^{-3}$
2	$.8725 \times 10^{-1}$	$.1153 \times 10^1$	.9804	$-.6000 \times 10^{-3}$
3	$.9525 \times 10^{-1}$	$.1103 \times 10^1$	.9843	$-.9500 \times 10^{-3}$
3	.1020	$.1103 \times 10^1$	.9843	$-.2500 \times 10^{-2}$
3	.1045	$.1103 \times 10^1$	.9843	$-.4700 \times 10^{-2}$
4	.1065	$.1031 \times 10^1$	.9884	$-.3600 \times 10^{-2}$
	.1080			
	.1095			
	.1115			
	.1145			
	.1230			
	.1291			
	.1304			
5	.1420	$.1114 \times 10^1$	.9850	$-.1900 \times 10^{-2}$
5	.1490	$.1114 \times 10^1$	.9850	$-.3400 \times 10^{-2}$
5	.1515	$.1114 \times 10^1$	.9850	$-.3500 \times 10^{-2}$
5	.1535	$.1114 \times 10^1$	.9850	$-.3300 \times 10^{-2}$
	.1550			
	.1565			
	.1580			
6	.1600	.9691	.9859	$-.1500 \times 10^{-2}$
6	.1657	.9691	.9859	$-.1500 \times 10^{-2}$
6	.1728	.9691	.9859	$-.1000 \times 10^{-2}$
	.1849			
	.1969			
	.2093			
7	.2224	.7011	.9657	$-.7200 \times 10^{-4}$
7	.2361	.7011	.9657	$-.7200 \times 10^{-4}$
7	.2503	.7011	.9657	$-.7200 \times 10^{-4}$

Table I. Continued

(c) Continued

Duct	X/c	p_{sc}/p_∞	$T_\infty/T_{t,sc}$	C_Q
8	0.2649	0.6892	0.9651	-0.7200×10^{-4}
8	.2800	.6892	.9651	$-.7200 \times 10^{-4}$
8	.2954	.6892	.9651	$-.7200 \times 10^{-4}$
8	.3112	.6892	.9651	$-.7200 \times 10^{-4}$
8	.3273	.6892	.9651	$-.7700 \times 10^{-4}$
8	.3437	.6892	.9651	$-.8000 \times 10^{-4}$
8	.3604	.6892	.9651	$-.8500 \times 10^{-4}$
9	.3772	.6884	.9651	$-.9200 \times 10^{-4}$
9	.3943	.6884	.9651	$-.9800 \times 10^{-4}$
9	.4115	.6884	.9651	$-.1050 \times 10^{-3}$
9	.4289	.6884	.9651	$-.1100 \times 10^{-3}$
10	.4463	.6942	.9661	$-.1170 \times 10^{-3}$
10	.4638	.6942	.9661	$-.1220 \times 10^{-3}$
10	.4814	.6942	.9661	$-.1300 \times 10^{-3}$
10	.4990	.6942	.9661	$-.1420 \times 10^{-3}$
11	.5165	.7124	.9677	$-.1550 \times 10^{-3}$
11	.5346	.7124	.9677	$-.1780 \times 10^{-3}$
11	.5515	.7124	.9677	$-.2000 \times 10^{-3}$
11	.5688	.7124	.9677	$-.2400 \times 10^{-3}$
12	.5860	.7368	.9694	$-.2800 \times 10^{-3}$
12	.6030	.7366	.9604	$-.3400 \times 10^{-3}$
13	.6197	.7434	.9734	$-.4100 \times 10^{-3}$
13	.6362	.7434	.9734	$-.1000 \times 10^{-2}$
14	.6526	.7949	.9800	$-.1920 \times 10^{-2}$
14	.6691	.7949	.9800	$-.1990 \times 10^{-2}$
15	.6857	.8364	.9855	$-.1830 \times 10^{-2}$
16	.7025	.8970	.9897	$-.1600 \times 10^{-2}$
17	.7198	.9812	.9922	$-.1390 \times 10^{-2}$
18	.7542	$.1019 \times 10^{1}$	.9937	$-.1270 \times 10^{-2}$
18	.7715	$.1019 \times 10^{1}$	.9937	$-.1360 \times 10^{-3}$
19	.7890	$.1073 \times 10^{1}$	.9953	$-.1570 \times 10^{-2}$
20	.8069	$.1096 \times 10^{1}$	.9965	$-.2100 \times 10^{-2}$
20	.8160	$.1096 \times 10^{1}$	.9965	$-.2500 \times 10^{-2}$
20	.8204	$.1096 \times 10^{1}$	.9965	$-.3000 \times 10^{-2}$
21	.8232	$.1064 \times 10^{1}$	.9965	$-.4200 \times 10^{-2}$
21	.8252	$.1064 \times 10^{1}$	.9965	$-.4700 \times 10^{-2}$
21	.8268	$.1064 \times 10^{1}$	.9965	$-.5000 \times 10^{-2}$
21	.8280	$.1064 \times 10^{1}$	.9965	$-.4500 \times 10^{-2}$

Table I. Concluded

(c) Concluded

Duct	X/c	p_{sc}/p_∞	$T_\infty/T_{t,sc}$	C_Q
	0.8292			
	.8304			
	.8316			
	.8332			
	.8349			
	.8369			
	.8386			
21	.8404	0.1064×10^1	0.9965	-0.1350×10^{-3}
21	.8421	$.1064 \times 10^1$	.9965	$-.6600 \times 10^{-3}$
21	.8438	$.1064 \times 10^1$	.9965	$-.1380 \times 10^{-3}$
21	.8458	$.1064 \times 10^1$	.9965	$-.2200 \times 10^{-2}$
21	.8475	$.1064 \times 10^1$	.9965	$-.3000 \times 10^{-2}$
21	.8491	$.1064 \times 10^1$	.9965	$-.3500 \times 10^{-2}$
21	.8503	$.1064 \times 10^1$	.9965	$-.3000 \times 10^{-2}$
	.8515			
	.8527			
	.8539			
	.8555			
	.8572			
	.8609			
	.8700			
	.8800			
	.8900			
	.9000			
	.9120			
	.9240			
	.9360			
	.9440			
	.9560			
	.9680			
	.9780			
	.9850			
	.9950			
	$.1000 \times 10^1$			
	$.1002 \times 10^1$			
	$.1008 \times 10^1$			
	$.1010 \times 10^1$			

Table II. Wake Drag Computations From Representative Theoretical Trailing-Edge Boundary-Layer Values on the Upper and Lower Surfaces of the Slotted LFC Airfoil

$[M_\infty = 0.82,\ \Lambda = 23°]$

(a) Theoretical trailing-edge boundary-layer parameters with full-chord laminar flow

R_c	$\frac{u_{e,\text{T.E.}}}{u_\infty}$	$\frac{U_{e,\text{T.E.}}}{U_\infty}$ †	$\frac{\theta_{uu}}{c}$	$\frac{\theta_{vu}}{c}$	$\frac{\delta_u^*}{c}$	$\frac{\delta_v^*}{c}$
Upper surface						
8×10^6	0.9168	0.9300	1.3820×10^{-4}	0.9484×10^{-4}	4.072×10^{-4}	2.782×10^{-4}
20			.8740	.5998	2.575	1.760
40			.6180	.4241	1.821	1.244
Lower surface						
8×10^6	0.8293	0.8576	0.8662×10^{-4}	0.8504×10^{-4}	1.842×10^{-4}	2.203×10^{-4}
20			.5479	.5378	1.165	1.393
40			.3847	.3803	.824	.985

† Equation (43).

(b) Representative wake drag coefficients computed with equations (29) and (38)

R_c	$c_{d,W}$ (eq. (29))	2nd term,‡ percent (eq. (29))	$c_{d,\text{total}}$ (eqs. (13) and (29))	$c_{d,W}$ (eq. (38))	$c_{d,\text{total}}$ (eqs. (13) and (38))
Upper surface					
8×10^6	1.771×10^{-4}	14	6.935×10^{-4}	2.072×10^{-4}	7.236×10^{-4}
20	1.120	14	5.171	1.310	5.361
40	.792	14	4.200	.926	4.334
Lower surface					
8×10^6	0.892×10^{-4}	22	7.946×10^{-4}	1.002×10^{-4}	8.056×10^{-4}
20	.564	22	6.056	.634	6.126
40	.399	22	4.988	.448	5.037

‡ The 2nd term consists of multiples of θ_{vu}.

Table III. Wake Drag Computations From Representative Theoretical Trailing-Edge Boundary-Layer Values on the Upper and Lower Surfaces of the Slotted LFC Airfoil Based on Coordinate Transformation of Equation (32)

$[M_\infty = 0.82,\ \Lambda = 23°]$

(a) Theoretical trailing-edge boundary-layer parameters with full-chord laminar flow

R_c	$\frac{\theta_{u_p u_p}}{c}$	$\frac{\theta_{v_p u_p}}{c}$	$\frac{\theta_{v_p v_p}}{c}$	$\frac{\delta^*_{u_p}}{c}$	$\frac{\delta^*_{v_p}}{c}$
Upper surface					
8×10^6	1.3350×10^{-4}	3.230×10^{-6}	3.061×10^{-5}	3.836×10^{-4}	4.979×10^{-5}
20	.8444	2.040	1.936	2.426	3.149
40	.5971	1.440	1.369	1.716	2.227
Lower surface					
8×10^6	0.8864×10^{-4}	-0.690×10^{-6}	0.745×10^{-5}	1.992×10^{-4}	-1.45×10^{-5}
20	.5606	−.440	.471	1.259	−.915
40	.3964	−.310	.333	.891	−.647

(b) Representative wake drag coefficients computed with equation (37)

R_c	$c_{d,W}$ (eq. (37))	3rd term,† percent (eq. (37))	$c_{d,\text{total}}$ (eqs. (13) and (37))
Upper surface			
8×10^6	1.553×10^{-4}	0.2	6.717×10^{-4}
20	.982	.2	5.033
40	.694	.2	4.102
Lower surface			
8×10^6	0.985×10^{-4}	0.08	8.039×10^{-4}
20	.623	.08	6.115
40	.441	.08	5.030

† The 3rd term consists of multiples of $\delta^*_{v_p}$.

Table IV. Design Streamline Boundary-Layer Profile Functions Used to Compute Wake Drag From Equation (45)

x_{tr}	$x_{\text{W.R.}}$	U_e/U_∞	$\delta^*_{u_p}$	$\theta_{u_p u_p}$	$c_{d,W}$
Upper surface					
0.90	1.094	0.9179	4.396×10^{-4}	3.045×10^{-4}	4.183×10^{-4}
.80			8.062	5.433	7.451
.76			8.752	5.870	8.048
.74			9.517	6.352	8.706
.67			13.58	8.845	12.10
.60			16.31	10.48	14.33
.55			20.11	12.68	17.32
.50			22.09	13.80	18.83
.45			25.07	15.46	21.08
Lower surface					
0.84	1.094	0.9191	2.703×10^{-4}	1.962×10^{-4}	2.715×10^{-4}
.75			3.265	2.360	3.265
.65			4.821	3.477	4.809
.55			8.502	6.089	8.419
.44			13.49	9.529	13.16
.20			26.91	18.39	25.36
.17			27.84	18.99	26.18
.07			28.78	19.62	27.05
.05			28.78	19.62	27.05

Table V. Variation of Boundary-Layer Transition Location Along Streamline Through Wake Rake and Wake Drag, With Reynolds Number for Optimum Slotted LFC Suction Data

	Upper		Lower		Total
R_c	Forward X/c	Aft X/c	Forward X/c	Aft X/c	$c_{d,W}$
10×10^6	$> 0.90^\dagger$	1.00	0.84	0.93	$6.7\text{–}8.3 \times 10^{-4}$
11	$> .90^\dagger$	1.00	.85	.97	7.0–8.2
12	.74	1.00	.89	.95	10.2–11.3
13	.60	.76	.64	.75	14.4–15.3
14	.53	.67	.54	.74	20.1–20.4
15	.55	.67	.17	.44	38.8–39.2
16	.55	.67	.17	.44	41.8
18	.52	.67	.17	.44	42.4–42.7
20	.52	.67	.04	.44	41.8–43.4

† Default transition at flap hinge.

Table VI. Theoretical Wake Drag Variation With R_c Based on Streamline Boundary-Layer Analysis at $R_c = 20 \times 10^6$ Rescaled to Test R_c on the Basis of $c_{d,W}\ R_c^{1/5}$ = Constant

Boundary-layer transition at upstream limit of detection								
	Upper surface			Lower surface			Total	
R_c	$(x/c)_{tr}$ ($R_c = 20 \times 10^6$)	$c_{d,W}$ ($R_c = 20 \times 10^6$)	$c_{d,W}$ (Rescaled)	$(x/c)_{tr}$ ($R_c = 20 \times 10^6$)	$c_{d,W}$ ($R_c = 20 \times 10^6$)	$c_{d,W}$ (Rescaled)	$c_{d,W}$ ($R_c = 20 \times 10^6$)	$c_{d,W}$ (Rescaled)
10×10^6	0.90†	4.2×10^{-4}	4.8×10^{-4}	0.84‡	2.7×10^{-4}	3.1×10^{-4}	6.9×10^{-4}	7.9×10^{-4}
11	.90†	4.2	4.7	.84‡	2.7	3.0	6.9	7.7
12	.74	8.7	9.6	.84‡	2.7	3.0	11.4	12.6
13	.60	14.3	15.6	.64	4.8	5.2	19.1	20.8
14	.53	17.9	19.2	.54	8.4	9.0	26.3	28.2
15	.55	17.3	18.3	.17	26.2	27.7	43.5	46.0
16	.55	17.3	18.1	.17	26.2	27.4	43.5	45.5
18	.52	18.2	18.6	.17	26.2	26.8	44.4	45.4
20	.52	18.2	18.2	.04	27.0	27.0	45.2	45.2

Boundary-layer transition at downstream limit of detection								
	Upper surface			Lower surface			Total	
R_c	$(x/c)_{tr}$ ($R_c = 20 \times 10^6$)	$c_{d,W}$ ($R_c = 20 \times 10^6$)	$c_{d,W}$ (Rescaled)	$(x/c)_{tr}$ ($R_c = 20 \times 10^6$)	$c_{d,W}$ ($R_c = 20 \times 10^6$)	$c_{d,W}$ (Rescaled)	$c_{d,W}$ ($R_c = 20 \times 10^6$)	$c_{d,W}$ (Rescaled)
10×10^6	0.90†	4.2×10^{-4}	4.8×10^{-4}	0.84‡	2.7×10^{-4}	3.1×10^{-4}	6.9×10^{-4}	7.9×10^{-4}
11	.90†	4.2	4.7	.84‡	2.7	3.0	6.9	7.8
12	.90†	4.2	4.7	.84‡	2.7	3.0	6.9	7.8
13	.76	8.0	8.7	.75	3.3	3.6	11.3	12.3
14	.67	12.1	13.0	.74	3.4	3.6	15.5	16.6
15	.67	12.1	12.8	.44	13.2	14.0	25.3	26.8
16	.67	12.1	12.6	.44	13.2	13.8	25.3	26.4
18	.67	12.1	12.3	.44	13.2	13.5	25.3	25.8
20	.67	12.1	12.1	.44	13.2	13.2	25.3	25.3

† Default transition at flap hinge.
‡ Default transition at end of suction.

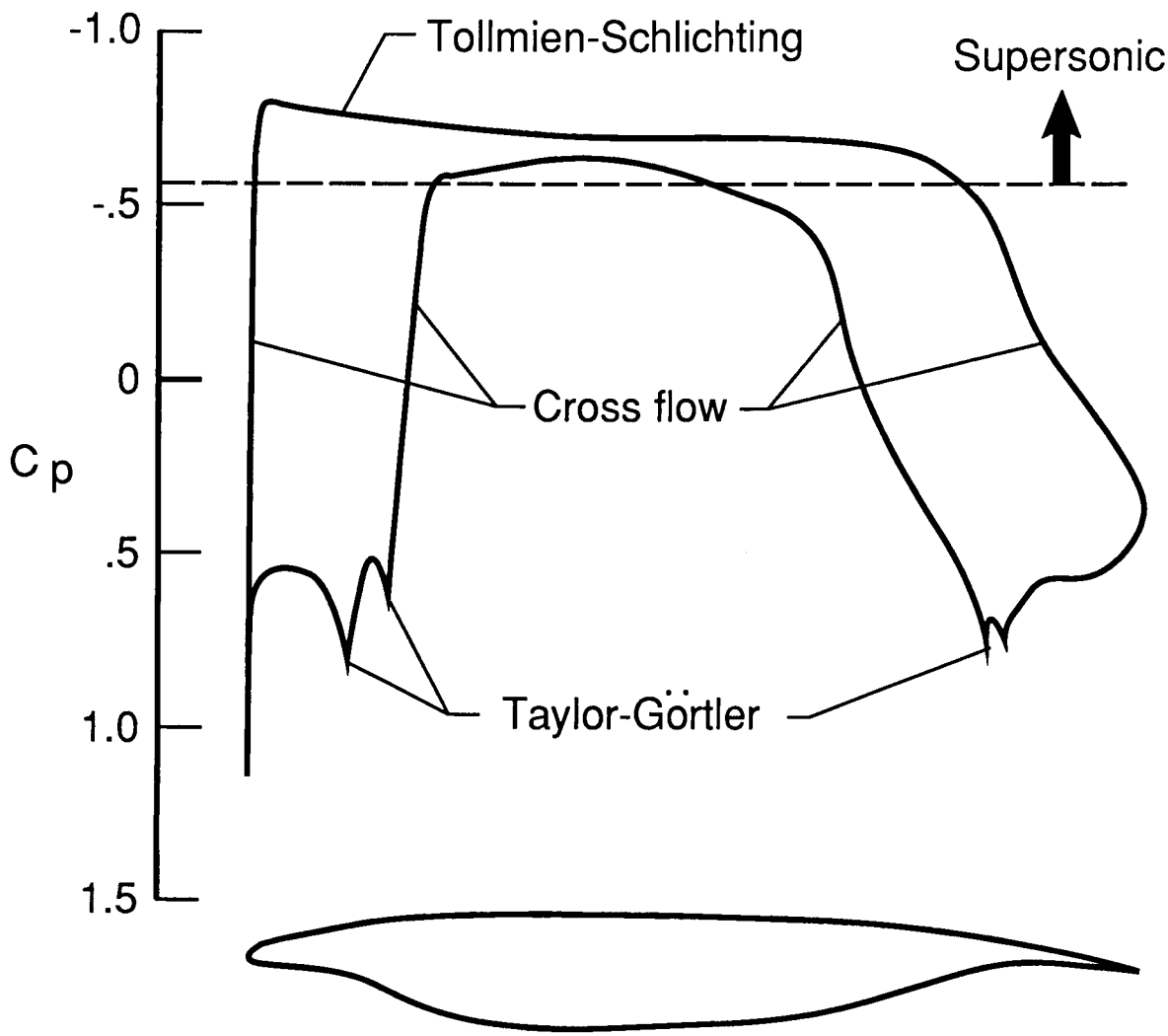

Figure 1. Airfoil geometry and pressure distribution (as computed by a 2-D compressible theory with $M = M_\infty \cos \Lambda = 0.755$) with indicated boundary-layer instability regions on a swept, supercritical LFC airfoil $c_l = 0.55$; $M_\infty = 0.82$; $\Lambda = 23°$.

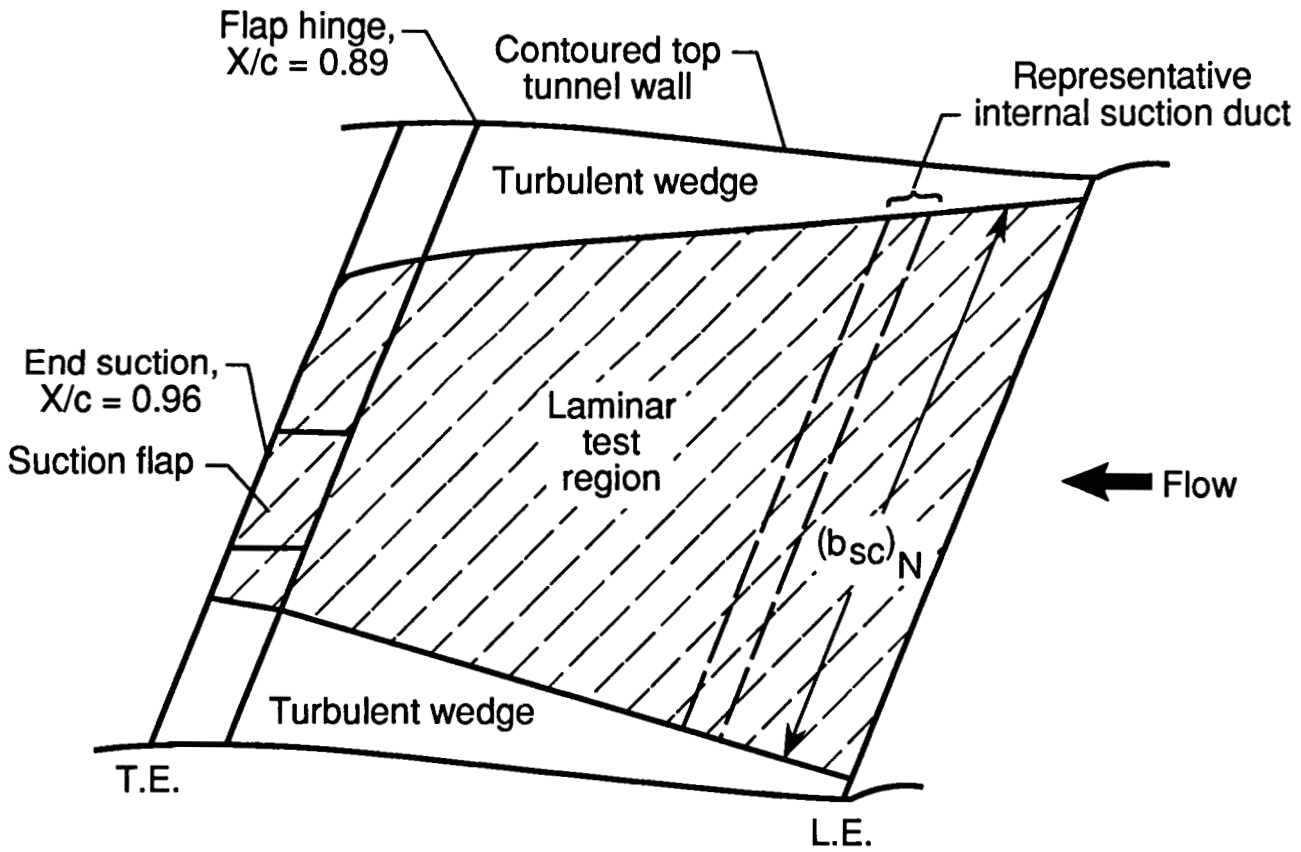

(a) Upper-surface test region.

Figure 2. Sketch of LFC airfoil laminar test region with suction (hatched region).

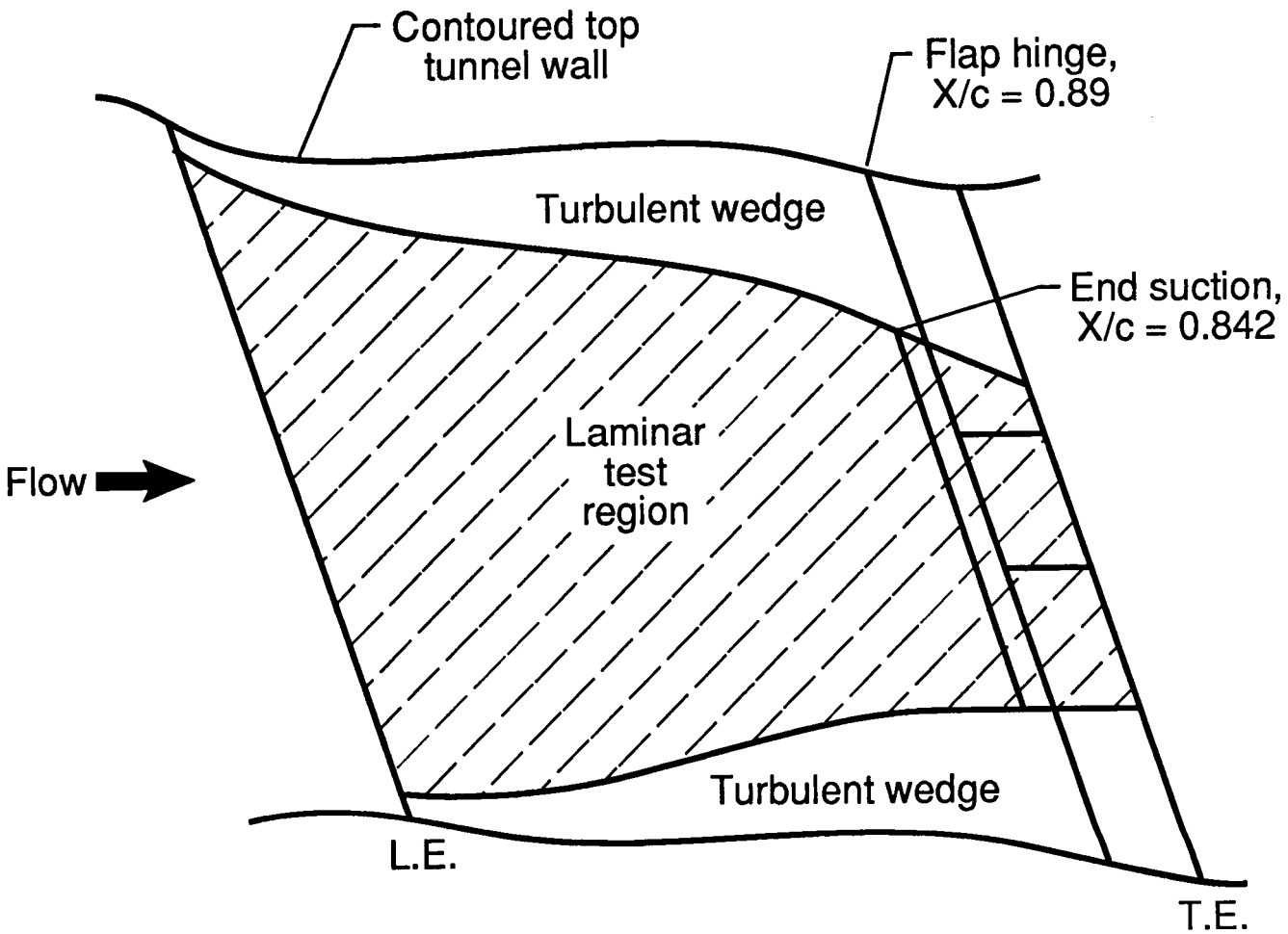

(b) Lower-surface test region.

Figure 2. Continued.

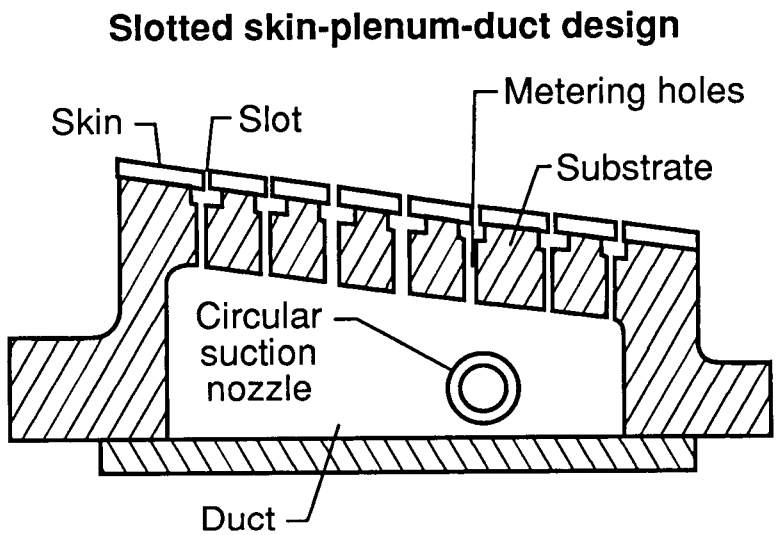

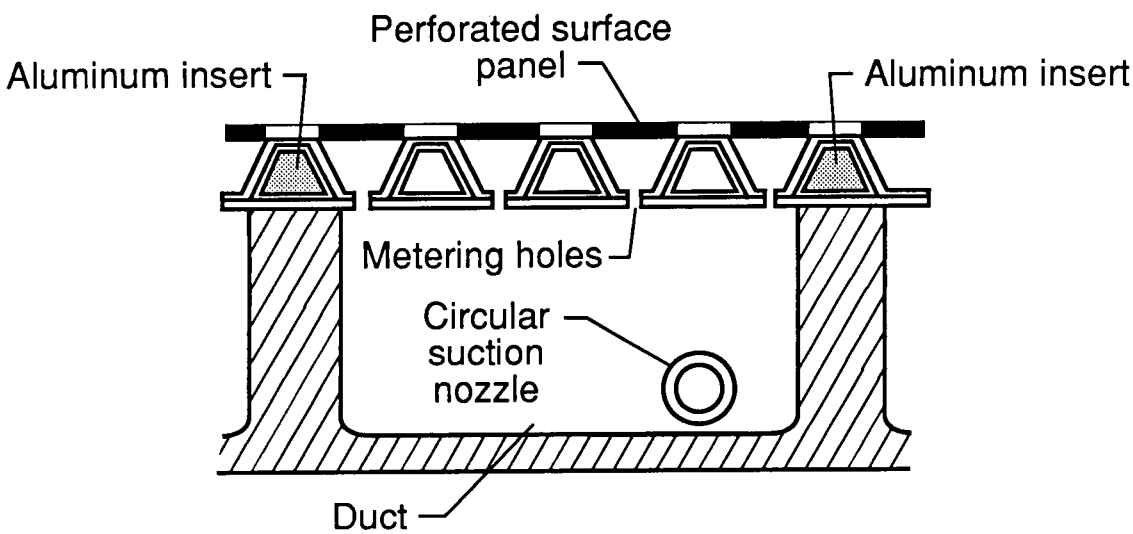

(c) Suction system design cross sections.

Figure 2. Concluded.

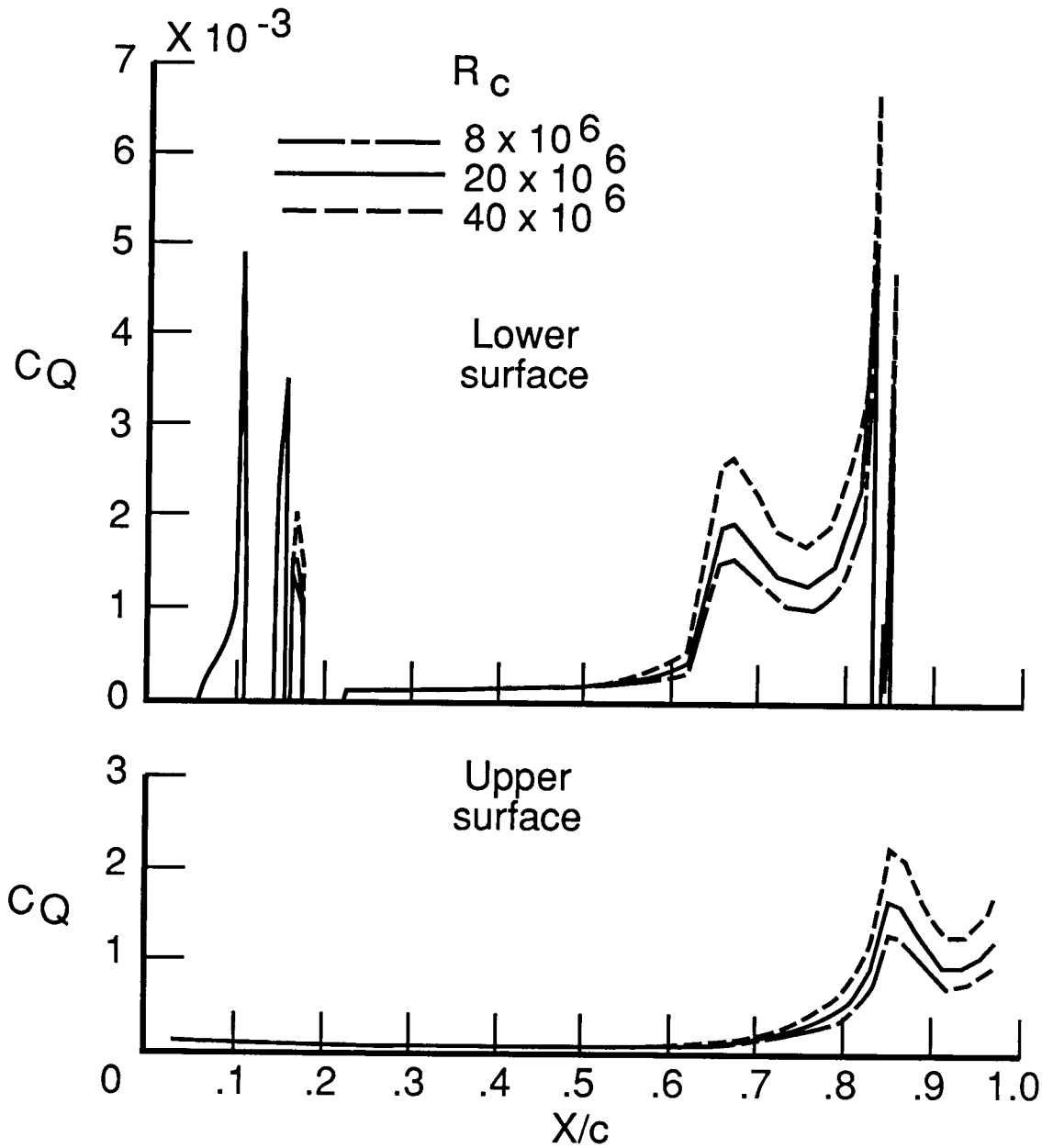

Figure 3. Theoretical variation of suction coefficient along chord for full-chord laminar flow over LFC airfoil at design condition. $c_l = 0.55$; $M_\infty = 0.82$; $\Lambda = 23°$.

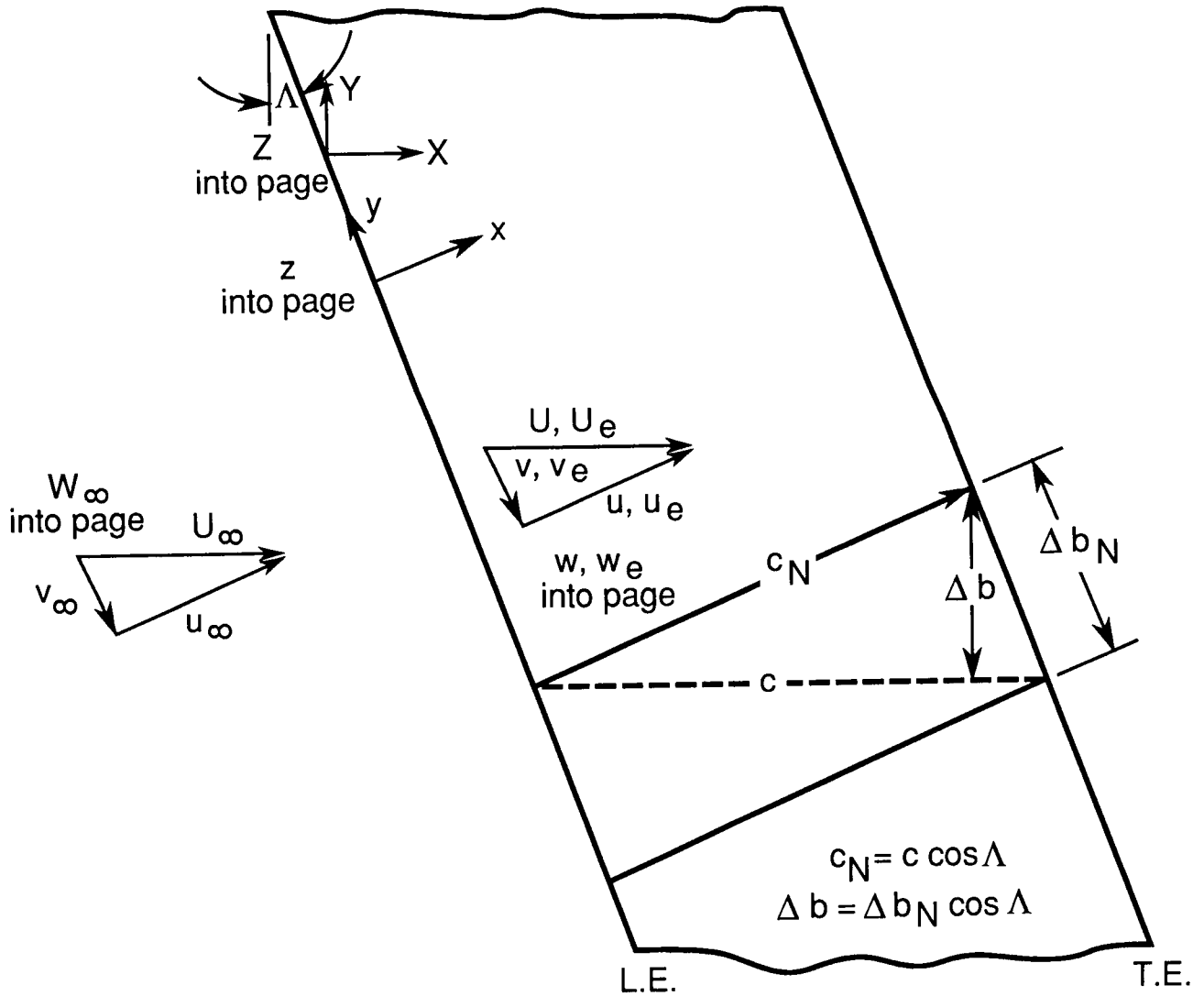

Figure 4. Flow analysis coordinate systems.

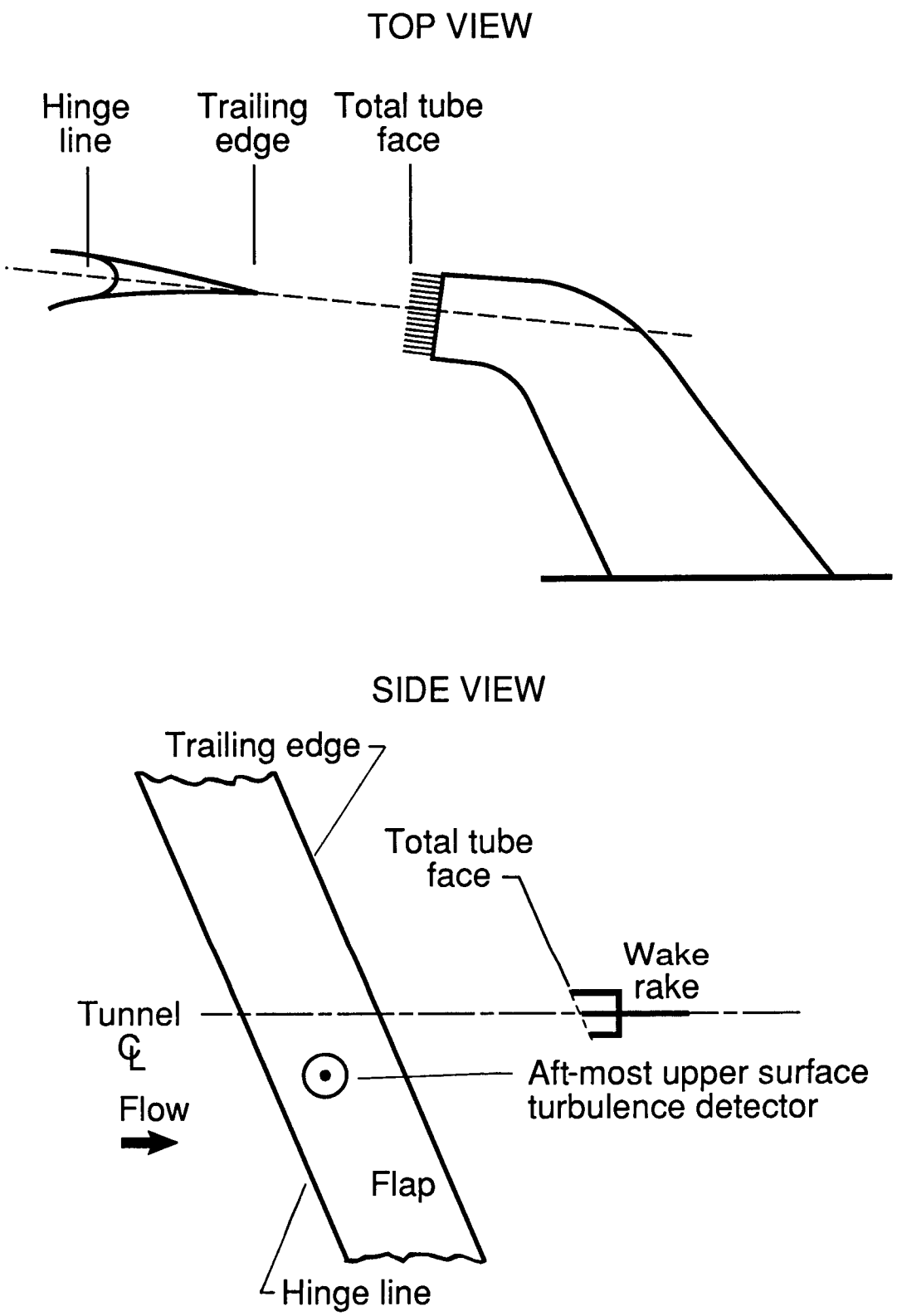

Figure 5. Schematic showing orientation of wake rake to LFC airfoil in the 8-ft TPT.

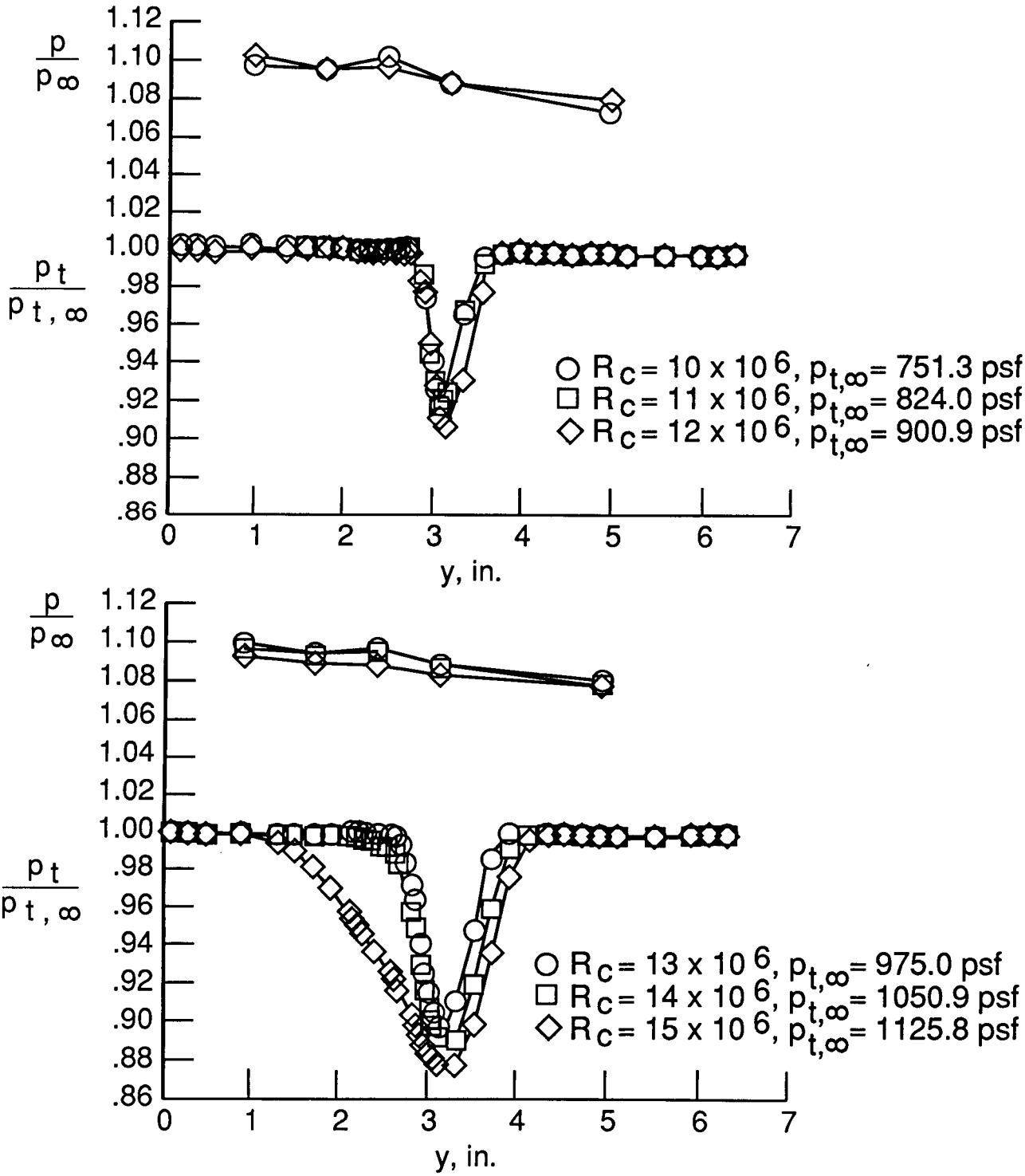

Figure 6. Typical variation of wake-rake static and total pressure ratios across wake ($y = 0$ on lower surface side) of swept LFC airfoil at design Mach number.

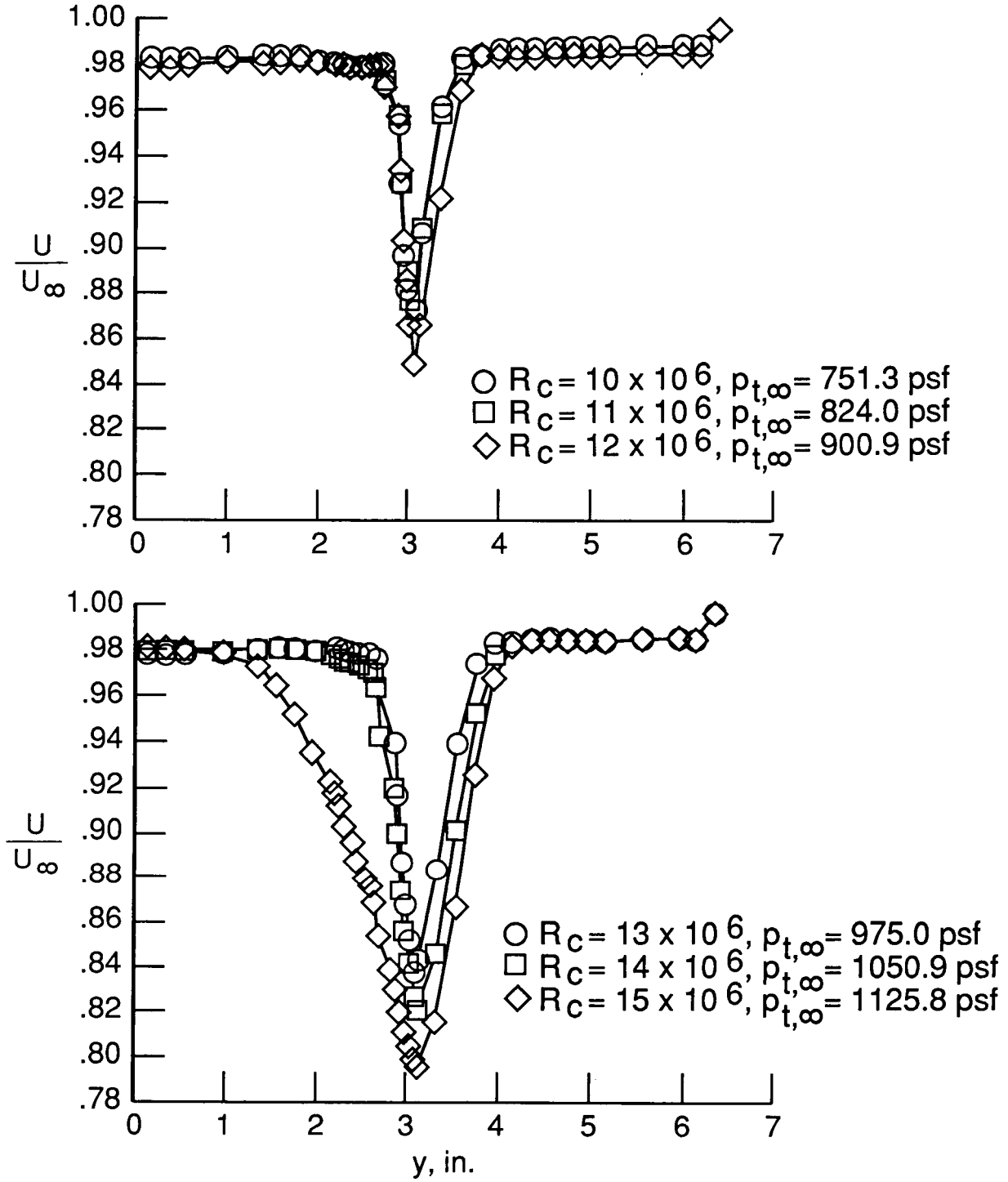

Figure 7. Typical variation of wake velocity ratio across wake ($y = 0$ on lower surface side) of swept LFC airfoil at design Mach number.

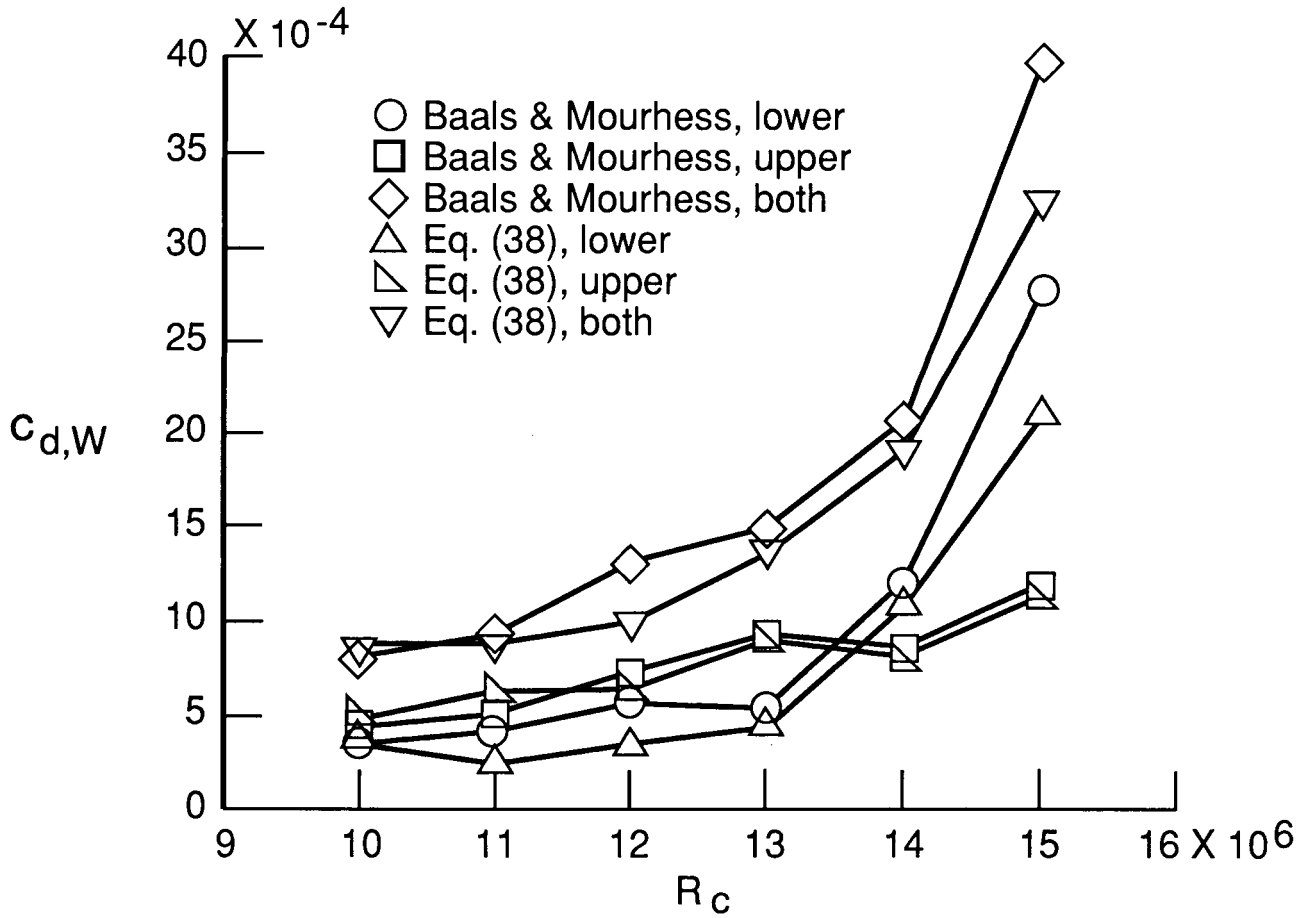

Figure 8. Comparison of typical wake drag coefficient variation with chord Reynolds number as computed from equation (38) with that computed by the Baals and Mourhess (ref. 2) 2-D method.

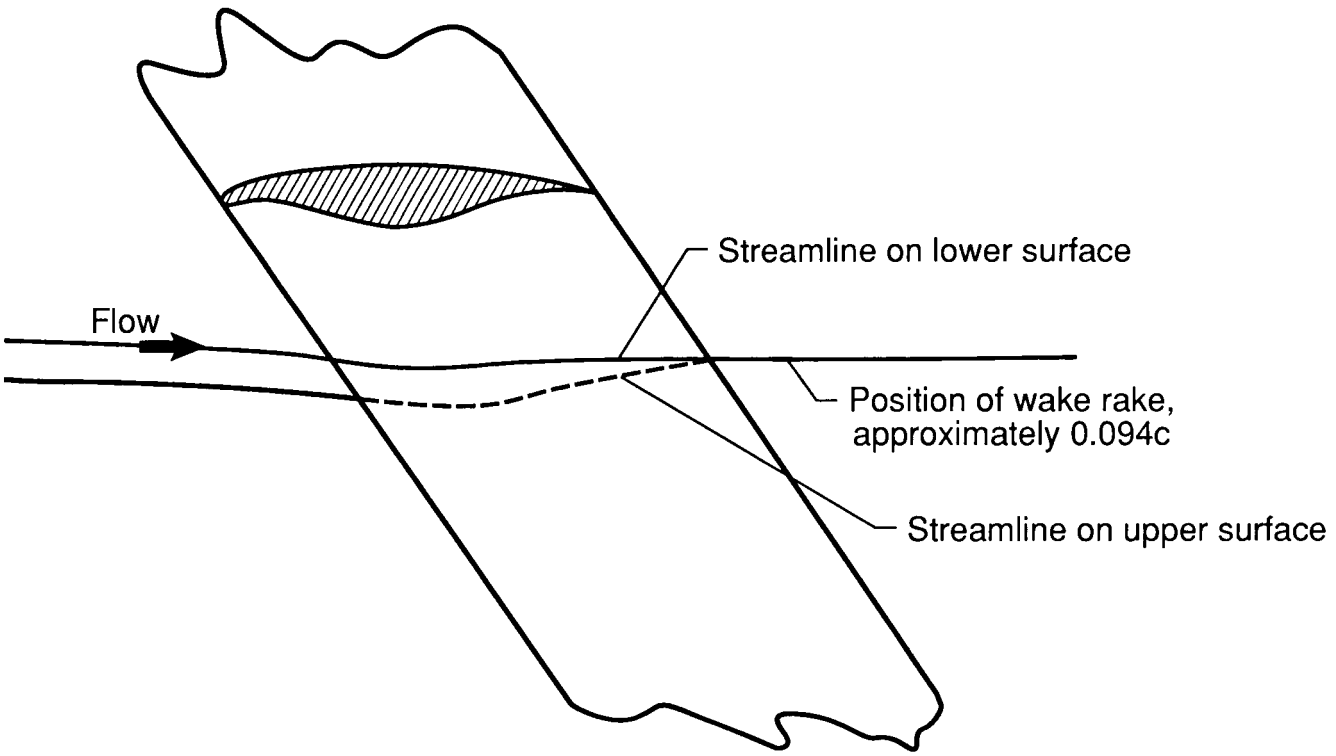

(a) Theoretical design streamlines converging at wake rake.

Figure 9. Computation of slotted LFC airfoil wake drag from theoretical streamline boundary layer using limiting experimental transition locations.

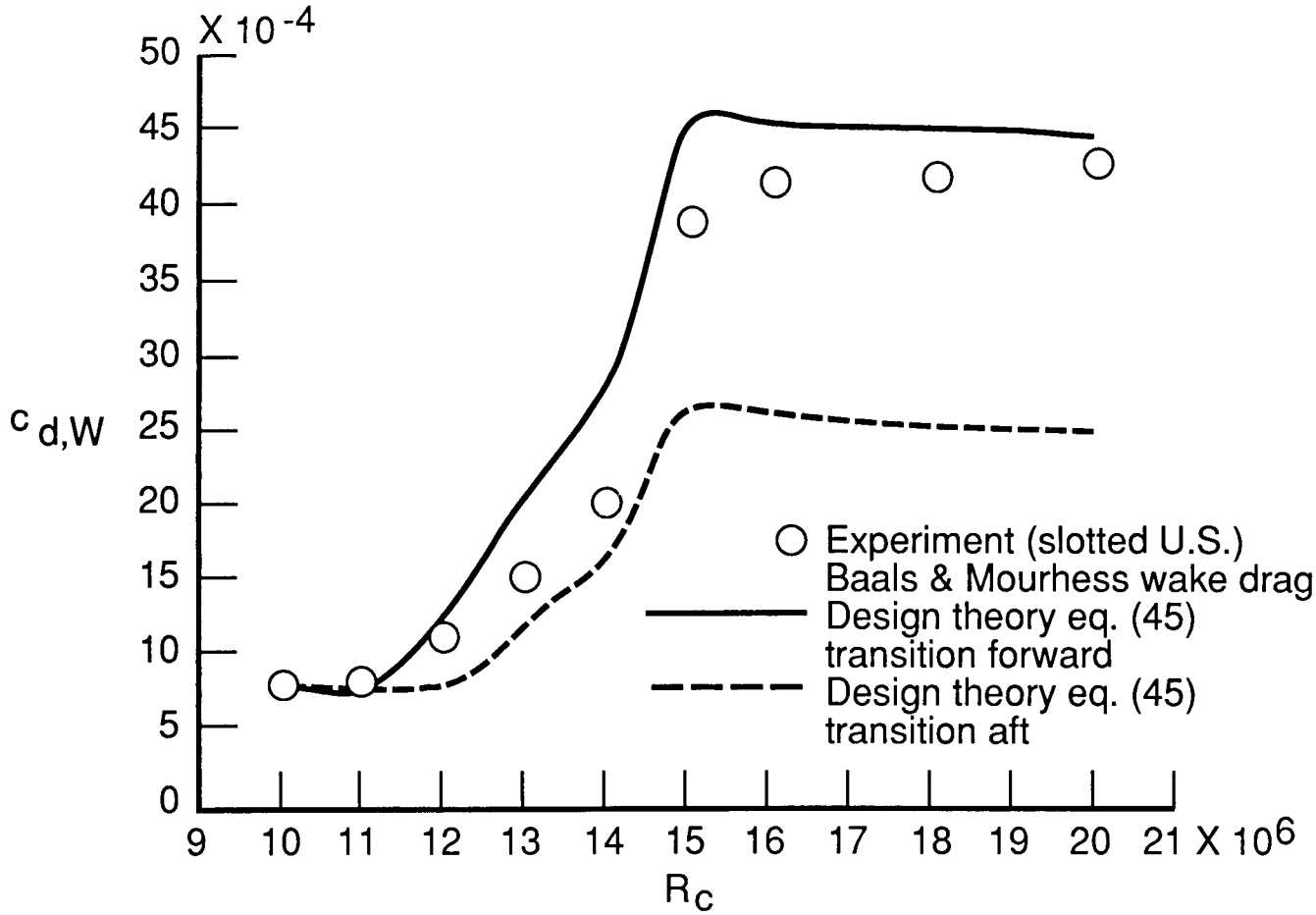

(b) Comparison of theoretical wake drag with experiment.

Figure 9. Concluded.

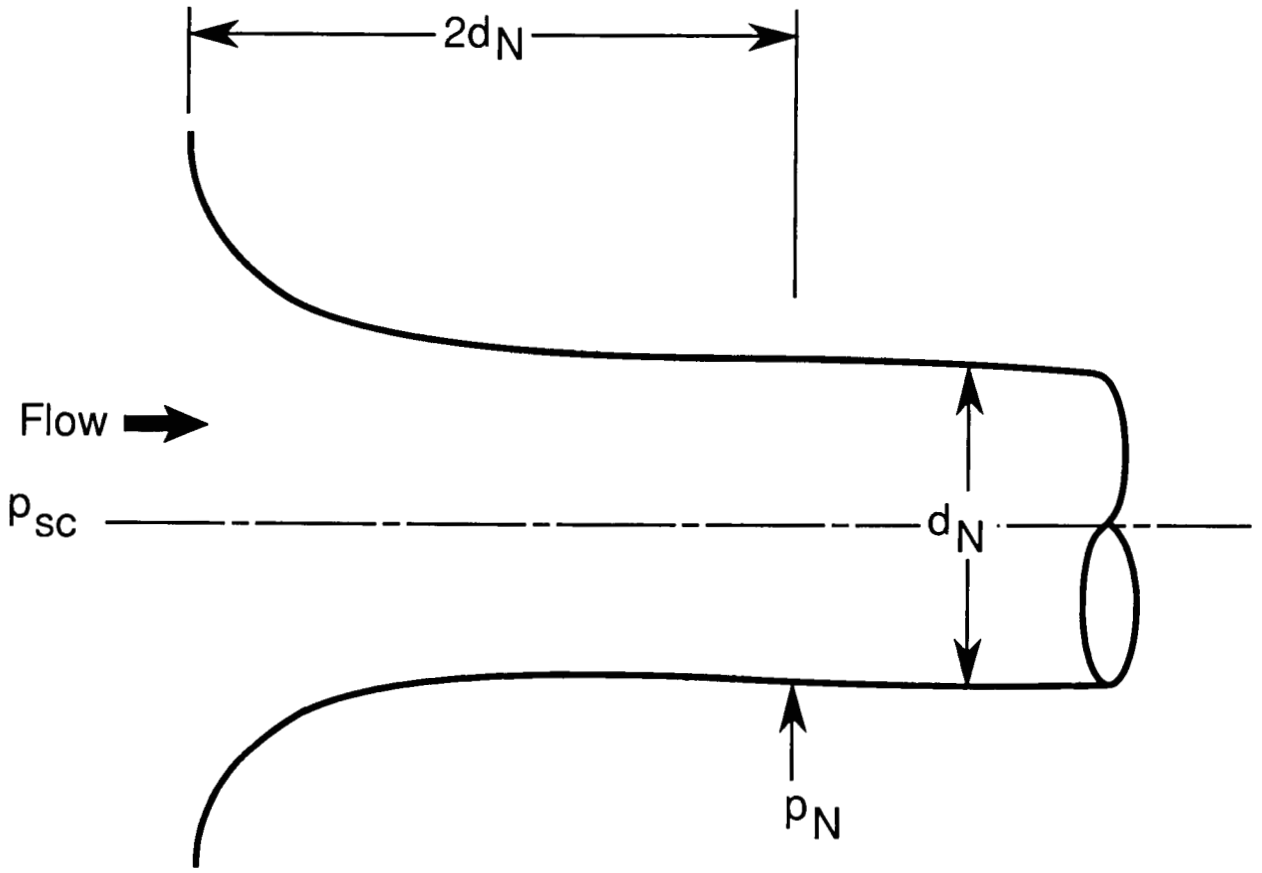

Figure 10. Sketch of calibrated suction nozzle.

NASA
National Aeronautics and Space Administration

Report Documentation Page

1. Report No.	2. Government Accession No.	3. Recipient's Catalog No.
NASA TM-4096		

4. Title and Subtitle	5. Report Date
The NASA Langley Laminar-Flow-Control Experiment on a Swept, Supercritical Airfoil—*Drag Equations*	March 1989
	6. Performing Organization Code
7. Author(s)	8. Performing Organization Report No.
Cuyler W. Brooks, Jr., Charles D. Harris, and William D. Harvey	L-16322
9. Performing Organization Name and Address	10. Work Unit No.
NASA Langley Research Center Hampton, VA 23665-5225	505-60-31-03
	11. Contract or Grant No.
12. Sponsoring Agency Name and Address	13. Type of Report and Period Covered
National Aeronautics and Space Administration Washington, DC 20546-0001	Technical Memorandum
	14. Sponsoring Agency Code

15. Supplementary Notes

16. Abstract

The Langley Research Center has designed a swept, supercritical airfoil incorporating laminar-flow control (LFC) for testing at transonic speeds. Analytical expressions have been developed and an evaluation has been made of the experimental section drag, composed of suction drag and wake drag, using theoretical design information and experimental data. The analysis shows that, although the sweep-induced boundary-layer cross-flow influence on the wake drag is too large to be ignored and there is not a practical method for evaluating these cross-flow effects on the experimental wake data, the conventional unswept two-dimensional wake-drag computation used in the reduction of the experimental data is at worst 10 percent too high.

17. Key Words (Suggested by Authors(s))	18. Distribution Statement
Laminar-flow control Swept, supercritical airfoil Suction	Unclassified—Unlimited Subject Category 02

19. Security Classif. (of this report)	20. Security Classif. (of this page)	21. No. of Pages	22. Price
Unclassified	Unclassified	40	A03

NASA FORM 1626 OCT 86

NASA-Langley, 1989

For sale by the National Technical Information Service, Springfield, Virginia 22161-2171